



FCTUC FACULDADE DE CIÊNCIAS
E TECNOLOGIA
UNIVERSIDADE DE COIMBRA

Electric sensor to investigate ablation and associated processes in thermal protection systems

Tiago Manuel de Oliveira Marques

Dissertação para obtenção do Grau de Mestre em
Astrofísica e Instrumentação para o Espaço

Júri

Presidente: Professor João Manuel de Moraes Barros Fernandes

Vogal: Professora Maria Alexandra Albuquerque Faria Pais

Orientadores: Professor José Lopes Pinto da Cunha

Engenheiro Abel Borges Ferreira Mendes

Outubro de 2013

Abstract

In this thesis is presented a non-invasive sensor to measure in real time the ablation of thermal protection systems during atmospheric entry and re-entry.

Thermal protection systems are critical to ensure that future spacecraft have the capabilities needed to descend through another planet atmosphere. One of the next challenges in space achievements is to send humans to Mars. For this type of mission it is useful to have a sensor measuring the recession rate of the thermal protection system and sending the data back to Earth.

The return from space incurs the risk of human casualties and property damages. The models used to assess this risk contain a large degree of uncertainty and lack experimental data for calibration. The data recorded is expected to provide invaluable insight leading to thermal protection systems optimization. Such sensor could reduce developmental costs and risks to space flight.

This electrical sensor is inspired in mutual impedance technique, suitable to measure the shield thickness during ablation.

Keywords: Thermal Protection Systems, Space Instrumentation, Atmospheric Entry, Mutual Impedance, Ablation, Electric sensors.

Resumo

Nesta tese, é apresentado um sensor não-intrusivo para medir, em tempo real, a ablação de um sistema de proteção térmica, durante uma entrada atmosférica.

Os sistemas de proteção térmica são indispensáveis para garantir que veículos espaciais possam aterrar noutros planetas. O próximo grande passo da humanidade ao nível espacial é enviar humanos para Marte. Para uma missão desse género, será fundamental ter um sensor que consiga medir a perda de massa em tempo real e que esses dados sejam enviados para a Terra.

O regresso do espaço é um risco para todos os tipos de missões, quer sejam tripuladas ou não tripuladas. Os modelos utilizados para estudar o risco necessitam de um grande volume de dados experimentais para refinar as calibrações e serem mais precisos. Espera-se que os dados recolhidos pelo sensor sejam de grande valor para a otimização dos sistemas de proteção térmica. Este sensor pode reduzir os custos e os riscos destas missões.

Este sensor usa a técnica da impedância mútua para medir a espessura da proteção térmica durante o processo ablativo.

Palavras Chave: Sistemas de proteção térmica, instrumentação para o espaço, entrada atmosférica, impedância mútua, ablação, sensores elétricos.

Contents

Abstract.....	iii
Resumo	iv
Acknowledgements	viii
List of Tables	x
List of Figures.....	xi
List of Acronyms.....	xiii
List of Symbols.....	xiv
1. Introduction	1
1.1. Motivation	1
1.2. Scope of the work	2
2. Theoretical Background	3
2.1. Atmospheres	3
2.2. Thermal Protection Systems	4
2.3. Ablative Materials.....	6
2.4. Ablation	6
2.5. CFD methods for ablating systems	8
3. State of the Art	10
Recession Measurement	10
3.1. ARAD	11
3.2. HEAT.....	12
4. The TPIP Project.....	14
4.1. Thermal Protection system sensor based on Impedance Probe (TPIP)	14
4.2. System Architecture.....	14
4.3. Mutual Impedance Probe	16
4.4. Electrodes Integration	19

5. Test Results	22
5.1. Electrodes Configuration Selection	22
5.2. Tested features	26
6. Conclusions	51
6.1. Thesis Contribution.....	51
6.2. Looking Forward	52
6.3. Future Work	52
6.4. Final Thoughts	52
Annexes	54
A1. P50 data sheet	54
A2. Calcarb data sheet	55
A3. System Requirements	56
References	58

Acknowledgements

The author wishes to acknowledge to all who have directly or indirectly assisted in the creation of this work:

First of all, thanks to my family, for the unconditional support. My heartfelt thanks to my mother, for the encouragement and permanent belief in me.

To Ricardo Patrício and Abel Mendes at Active Space Technologies, for accepting me to do my master dissertation while doing an internship at the company. I learned a lot with all AST team. Special thanks to Fernando Simões, for his invaluable insights and transmitted passion about science.

Prof. José Pinto da Cunha and Prof. João Fernandes at University of Coimbra, for advising me to make my thesis in a company.

And last, but not least, my good friends for keeping me sane and enjoying life.

List of Tables

Table 1: Orders of magnitude of anticipated recession for each type of mission.	5
Table 2: Different electrode configurations [29].....	25
Table 3: Dielectric properties of tested materials.....	27
Table 4: Calibration of TPIP sensor. Data acquired at the frequency of 1 kHz and using cables of 38 cm of length.....	28
Table 5: Number of time a configuration appears among the best configurations for each frequency.	35
Table 6: Average and standard deviation of TPIP measurements for configuration 4: PCB vs. SP electrodes.	50
Table 7: Functional Requirements.....	56
Table 8: Performance Requirements.	56
Table 9: Environmental and Operational Requirements.	56
Table 10: Physical Requirements.	56
Table 11: Design Requirements and Implementation Constraints.	56

List of Figures

Figure 1: Artist impression of a spacecraft atmospheric reentry [32].	3
Figure 2: ARD Front-shield TPS a) before and b) after recovery [4].	6
Figure 3: Ablation Process [24].	7
Figure 4: Surface Mass Balance (SMB).	9
Figure 5: Surface Energy Balance (SEB).	9
Figure 6: Schematics of Arad sensor. Each ARAD device consists of a narrow rod made of the ablator material itself (carbon fiber phenolic) wrapped with alternating layers of insulating tape (Kapton), Platinum-Tungsten wire, another Kapton layer, and Nickel ribbon [25].	11
Figure 7: Heat Sensor. a) materials [26], b) schematics [27].	13
Figure 8: TPIP system architecture.	15
Figure 9: Electrodes assembly [1] a) Electrodes view b) Shielding view.	16
Figure 10: Principle of Mutual Impedance measurement [29].	17
Figure 11: P50 sheets from Amorim Cork Composites.	18
Figure 12: 1 - Ablative TPS layer; 2 - Internal layer. Adapted from [23].	19
Figure 13: Integration of the electrodes in the internal surface of TPS. In black is shown the wire used for the signals transmission between the electrodes and the data acquisition unit.	20
Figure 14: Characterization of all 10 different electrode configurations measuring P50 samples. FR4 is an epoxy based composite present on printed circuit boards (PCB) and is where the electrodes are integrated.	29
Figure 15: Mean and standard deviation of the amplitude and phase as a function of thickness at 10 Hz [29].	30
Figure 16: Mean and standard deviation of the amplitude and phase as a function of thickness at 200 Hz [29].	31
Figure 17: Mean and standard deviation of the amplitude and phase as a function of thickness at 1kHz [29].	32
Figure 18: Mean and standard deviation of the amplitude and phase as a function of thickness at 10 kHz [29].	33

Figure 19: Mean and standard deviation of the amplitude and phase as a function of thickness at 100 kHz [29].	34
Figure 20: Electric field representation.	36
Figure 21: influence of DC electric field on TPIP measurements. The vertical dashed line identifies when the electric field is turned on [29].	37
Figure 22: Magnetic field test assembly.	38
Figure 23: Influence of a DC magnetic field on TPIP measurements [29].	38
Figure 24: Equipotential test setup.	39
Figure 25: Electric field distribution with (bottom) and without (top) an equipotential surface [28].	40
Figure 26: Amplitude and phase as function of thickness with and without equipotential surface [29].	41
Figure 27: Thermal chamber test [29].	42
Figure 28: Influence of temperature on amplitude and phase measurements. Results for a P50 sheet of 5 mm thick [29].	42
Figure 29: P50 burning [1].	43
Figure 30: Influence of heat and pyrolyzation on TPIP measurements. P50 with thickness of 10 mm [29].	44
Figure 31: Testing TPIP response to thickness increase with Calcarb® layers. Note that the sensor is attached to a P50 plate with 5 mm thick [1].	45
Figure 32: Amplitude and phase as a function of thickness at frequency of 1 kHz [29].	46
Figure 33: Calcarb burning [1].	46
Figure 34: Influence of heat and pyrolyzation on TPIP measurements - Calcarb® with thickness of 18 mm [29].	47
Figure 35: Influence of heat and pyrolyzation on TPIP measurements. P50 - 5 mm and Calcarb® - 18 mm [29].	48
Figure 36: Silver Paint electrodes painted on a P50 plate. Same geometry as configuration four (C4).	49
Figure 37: Amplitude and phase as a function of thickness vs. silver paint electrode [29].	50
Figure 38: MI signal at 1 kHz as function of P50 thickness.	53

List of Acronyms

ARAD	Analog Resistance Ablation Detector
ARD	Atmospheric Reentry Demonstrator
AST	Active Space Technologies
CFD	Computational Fluid Dynamics
ELF	Extreme Low Frequency
ESA	European Space Agency
FFT	Fast Fourier Transform
HEAT	Hollow aErothermal Ablation Temperature
IS	Impedance Spectroscopy
IXV	Intermediate eXperimental Vehicle
MEDLI	Mars Science Laboratory Entry, Descent, and Landing Instrument
MI	Mutual Impedance
MIP	Mutual Impedance Probe
MSL	Mars Science Laboratory
NASA	National Aeronautics and Space Agency
PCB	Printed Circuit Board
PVD	Physical Vapor Deposition
TPIP	Thermal Protection System sensor based on Impedance Probe
TPS	Thermal Protection System
VLF	Very Low Frequency

List of Symbols

A Amplitude

E Electric field

f Frequency

I Current

R Resistance

Z Impedance

ϵ Permittivity

σ Conductivity

φ Phase

ω Angular frequency



Introduction

1.1. Motivation

Space vehicles that enter a planetary atmosphere require use of a thermal protection system (TPS) to shield them from aerodynamic heat. The TPS consists of various materials applied on the spacecraft to give protection against aerodynamic heating. This, combined with vehicle's configuration and entry trajectory, define the temperature distribution on the vehicle. The problem of re-entry on the Earth's atmosphere was a significant challenge for the early spaceflight researchers, as they considered how best to overcome the heat resulting from friction and compression of the atmospheric gas. Nowadays, the research challenge is more focused on TPS optimization, to improve material performance and risk assessment.

Investigation of ablation processes on the surface of TPS during entry or re-entry in the atmosphere is fundamental for humans to go further in space exploration. The term ablation is usually referred to the removal of material from the heat shield due to material heating and pyrolysis, which is caused by atmospheric gas drag. For any planetary entry probe, the heat shield is a key component that can constitute a significant fraction of the available spacecraft mass and respective mass budget. The lack of in-flight data from previous missions does not allow the reduction of uncertainties about mass constraints, and it is essential to develop lightweight techniques and in-situ sensors to assess the interaction between the aerothermodynamic flow and the TPS response. The performance of TPS ablation is closely related to the mass and heat transfer as well as to chemical reactions that occur within the gas boundary layer. Usually, heat shield mass is overestimated to increase re-entry safety margins.

1.2. Scope of the work

The project presented and discussed in this thesis aims to develop an innovative non-intrusive electrical sensor to provide real time measurements of the TPS surface recession of entry and re-entry space vehicles. This research was conducted during an 8 months internship at the Active Space Technologies, in Coimbra. The first phase of the project has been completed and delivered to the client (ESA). The executive summary is already available [1] and this work resulted in a patent [2] with the author as a co-inventor.

For terrestrial missions, the amount of mass lost can sometimes be analyzed after landing, the same is not possible for planetary missions. Nevertheless, it is very important to study the ablation during re-entry, when ablation processes are most critical.

TPIP sensor is based on Mutual Impedance technique and will allow an accurate measurement of shield thickness during re-entry, by means of a non-intrusive electrical method. It is based on a mutual impedance probe used to measure the dielectric properties of the medium, and infer real time estimation of the TPS ablation during re-entry. The dielectric properties of most materials vary with frequency, composition, and temperature because polarization is also a function of those parameters.

Theoretical Background

2.1. Atmospheres

The atmosphere has an important role in the design of entry vehicles. It is responsible for reducing the entry velocity to an acceptable landing speed by converting kinetic energy to heat by friction and air compression. During the hypersonic flight within the atmosphere, depending on velocity and trajectory, the temperature around the spacecraft shield may surpass 2000 °C [30] (See Figure 1).

An atmosphere is a layer of gases that may surround a material body of sufficient mass, like a planet or moon. In our Solar System there are several planets and moons that have a substantial atmosphere.



Figure 1: Artist impression of a spacecraft atmospheric reentry [32].

2.2. Thermal Protection Systems

To protect the spacecraft structure from the high temperatures that are present during atmospheric entry or re-entry is mandatory to use a heat shield. The TPS is usually made of layers of various materials applied outside of the structure of the space vehicle to maintain the skin within a range of acceptable temperatures. The TPS mass depends primarily on spacecraft size, shape and the entry profile. The TPS can be divided in two broad classes: i) one uses a covering material that will absorb the heat and radiate it back into space, away from the spacecraft. In fact, all materials radiate heat depending of the temperature. However, only certain materials can radiate heat so efficiently that the temperature does not build up within the material and in the spacecraft, possibly melting its structure. ii) another class of TPS is intended to burn and fall away from the spacecraft. These materials need not absorb or radiate efficiently, so when the surface becomes very hot, the material starts to burn steadily and erodes. The term that describes this process of material being eroded by heat is ablation. This work mainly focus on ablative TPS, described more in detail in next section. Table 1 shows some predicted recession thickness taken from various missions [3]. All considered vehicles are capsules, except Intermediate eXperimental Vehicle (IXV).

Mission	Area	Material	Thickness	Recession
Advanced Re-entry Vehicle - 1998 [4]	Front Shield	Low Density Carbon-Phenolic	60 to 80 mm	10-20 mm
	Back Cover	Norcoat-Liège	10 to 15 mm	~ 2 mm
IXV - 2009 [5]	Windward	Low Density Carbon-Phenolic	80 to 100 mm	15-20 mm
	Leeward	Norcoat-Liège	12 to 19 mm	~ 0
Jupiter (Galileo) – 1989 [6]	Front Shield	High Density Carbon-Phenolic	140 (nose) to 55 mm (shoulder)	~ 45 mm
Titan (Huygens) – 1997 [7]	Front Shield	AQ60 (LD Silica Phenolic)	17 to 19 mm	< 2 mm
	Back Cover	Prozial	1 to 3 mm	0
Mars Express (Mars) – 2003 [8]	Front Shield	Norcoat-Liège	8 to 12 mm	1 – 2 mm
	Back Cover	Norcoat-Liège	1,5 to 8 mm	0

Table 1: Orders of magnitude of anticipated recession for each type of mission.

2.3. Ablative Materials

Different thermal protection systems (ablation, heat sink, transpiration cooling) have been proposed and studied quite extensively, especially from the experimental point of view. Among them, is ablative TPS, which is characterized by a sacrificial removal of the surface material to protect the underlying structure, are normally applied on spacecraft or solid rocket nozzles. When surface is hot enough the material starts burning and ablating, thus protecting the spacecraft. The process is explained in section 2.4. Ablative TPS must be designed to protect the vehicle with a minimum weight penalty. Typically, we categorize ablative TPS by density, i.e., low density, mid density and high density. Material strength increases with density, but so does the thermal conductivity. Depending on mission entry environment the selected material requires a balance between ablative and insulation efficiency. In Figure 2 is shown the result of ablation on Advanced Re-entry Vehicle (ARD).



Figure 2: ARD Front-shield TPS a) before and b) after recovery [4].

2.4. Ablation

A complete understanding of the ablation process however, requires a study of the heat loads experienced during the entry process. This is the most significant heat load. Radiative heat flux from the preceding bow shock also provide a significant heat load that contribute to the total and dictate which materials can be exposed to these loads.

Consequently, a combination of design strategy and understanding of the re-entry environment can be used to control ablation. Section 2.5 shows however, that current models used to simulate such an environment contain critical uncertainty.

During entry, ablative materials undergo three stages, as can be seen in Figure 3: i) virgin material, ii) pyrolysis¹ and iii) char. The material is considered virgin until it has been affected by heat or radiation as heating increases and pyrolysis begins. As it is heated, the original virgin material pyrolysis and yields a pyrolysis gas, which percolates away from the pyrolysis zone leaving a porous residue which for most materials it is a carbonaceous char. This char is low density substrate that adheres to the remaining material after the pyrolysis phase ends. The phenomena can be described as the process whereby mass is removed from an object by vaporization or other similar erosive processes. But the ablation also occurs in different branches of physics, for example, in the melting or sublimation of a solid or in laser drilling in metals and the cornea surgery [9].

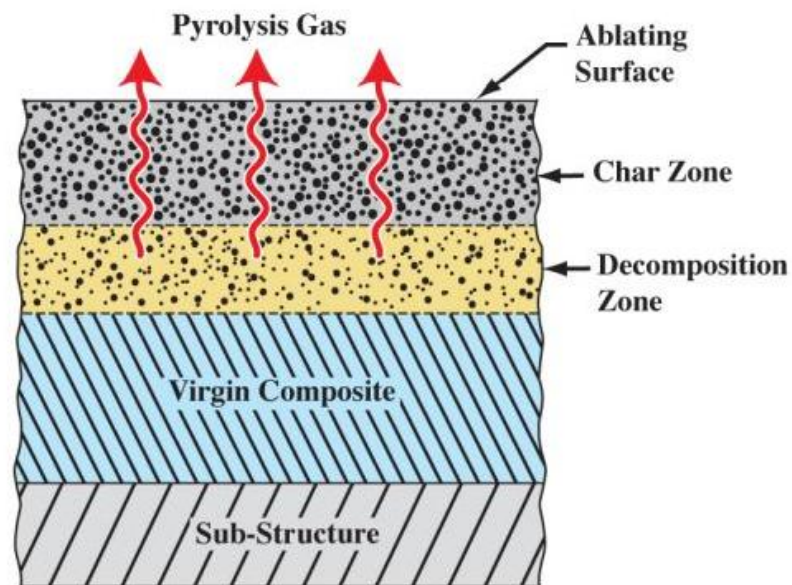


Figure 3: Ablation Process [24].

The ablation process is schematically represented in Figure 3, showing that when heated, the composite resin (epoxy) experiences a series of chemical reactions that release gaseous by products (pyrolysis) leaving a layer of char.

¹ Decomposition of organic material at high temperatures.

The study of ablative processes can be grouped in three main categories: i) engineering models, ii) numerical models and iii) experimental methods. Engineering models are recommended in the initial stages of space vehicles development; numerical models apply the theory and can predict the occurring processes; and experimental methods can give inputs to the other methods and validate some concepts.

2.5. CFD methods for ablating systems

Having an accurate prediction of the thermal response of TPS materials is essential to successfully carry out the design of an optimum TPS. Simulation tools should be able to compute the surface recession and temperature histories under general heating conditions. Most commercial Computational Fluid Dynamics (CFD) codes use ordinary surface boundary conditions and cannot be realistically used to predict the aerothermal heating profile of TPS [10]. Normally, CFD codes treat fluid/solid boundary conditions in a simplified approach and mass transfer is often not even considered. Current methods focus on some aspects of the problem at expense of others and simplifying the studies by making assumptions. Thus, aerodynamic methods concentrate on the flowfield, and rely on other methods to provide material-response characteristics; on the other hand, material-response methods concentrate on surface ablation and heat conduction in the material, using simplified models to provide the aerothermodynamic heating. However, to improve estimation of the heat flux over an ablating surface, a flow solver coupled with ablating surface conditions becomes a requirement. Aerothermodynamics phenomena on the receding surface ablate the material and induce electric currents in the shield. For aerothermal heating predictions over ablating TPS, is necessary to develop surface thermochemistry procedures that integrate with a Navier-Stokes flow solver. The general boundary conditions should include appropriate energy and multispecies mass balances with surface ablation models (See Figure 4 and Figure 5, source [11]).

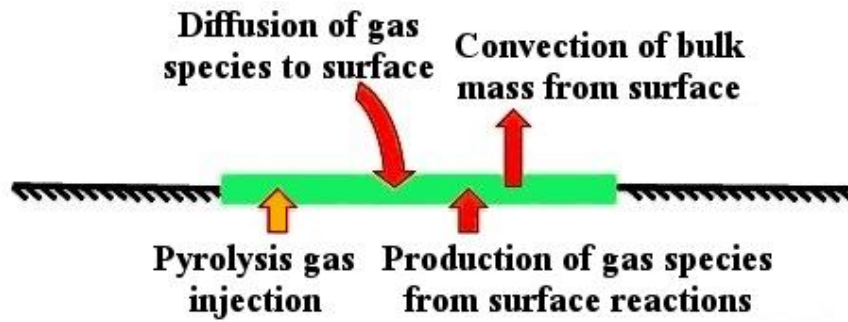


Figure 4: Surface Mass Balance (SMB).

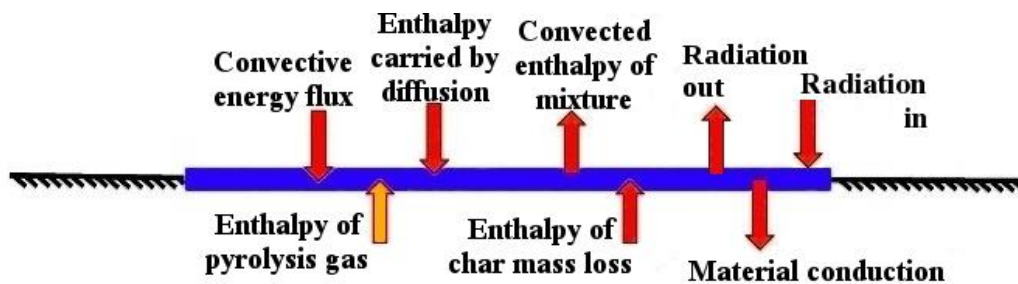


Figure 5: Surface Energy Balance (SEB).

Chemical reactions involving different enthalpy and phase changes take place at TPS wall, heating and removing material from the shield and modifying in-depth fluxes. Graphite is the simplest and the most popular material used to study ablation processes. Oxidation, nitrification, and sublimation are among the common processes that occur on the front shield.

The model presented above was used by *D. Bianchi* [12] to describe the ablation problem. Again, considering some assumptions:

- Steady-state flow;
- Negligible radiation heat transfer from the hot gas;
- Pyrolysis gas in chemical equilibrium at the wall temperature and pressure.

To formulate mathematically this problem it is necessary:

- Compressible Navier-Stokes equations;
- General heat-transfer equation;
- Mass transport equation;
- Equation of State;

A blue square graphic with the word "Chapter" written vertically in white on the left side and a large white number "3" in the center.

State of the Art

TPS Recession is currently measured on probes using namely one of two sensor types: the Analog Resistance Ablation Detector (ARAD) [13], and the Hollow aErothermal Ablation Temperature detector (HEAT). These are the two most common types of sensors that have been used to measure recession.

Recession Measurement

Recession is the term used to define the amount of TPS material ablated during entry and recession measurements shows how the TPS shield mass change in the process of entry. In situ TPS sensors are required to provide optimization: sizing tools, design, and material performance, leading to risk reduction and decrease of mass requirements.

Information about the total recession is quite limited on Earth and practically non-existent in other planetary missions though, the Galileo mission showed that temperature and recession measurements contributed to a better understanding of the Jupiter entry environment and will contribute to improve TPS architectures in future missions [14]. Recession is generally quite low for most planetary entries, with the exception of Galileo probe entry in Jupiter atmosphere (See Table 1). Manned vehicles require more stringent safety conditions, consequently, the TPS thickness and estimated ablation of such spacecraft ought to be higher.

A four-electrode array employing the mutual impedance technique was used on board the Huygens Probe to measure the dielectric properties of Titan surface and the conductivity of the atmosphere.

3.1. ARAD

One of the more successful efforts in the development of a surface recession sensor is the quartz-based Analog Resistance Ablation Detector (ARAD), originally developed by General Electric [15]. The NASA probe heat shield was instrumented with ARADs to monitor the probe's heat shield deformation and mass loss during its entry into Jupiter's atmosphere (Galileo mission) [13]. The operating principle was similar as the quartz-based ARAD but used different materials. The ARAD sensors were comprised of a narrow (~2mm diameter) rod of carbon phenolic (forebody material) wrapped with alternating layers of insulating tape (Kapton), Platinum-Tungsten wire, more insulating tape, and Nickel ribbon [15] (see Figure 6). The resistance of the Platinum-Tungsten wire was much higher compared to that of the Nickel. The ARAD operative principle is based on the fact that the char produced by the ablating phenolic and Kapton is electrically conductive. An electronic circuit supplies a constant current, as excitation; the Platinum-Tungsten wire, char and phenolic loop complete the circuit. The voltage is measured across Nickel sensing wire and the Platinum-Tungsten wire. As the phenolic gets ablated, the Platinum-Tungsten wire is shortened decreasing the resistance. Arc jet² testing demonstrated a resolution of 0.09 cm recession, for a maximum 0.1 cm/s recession rate.

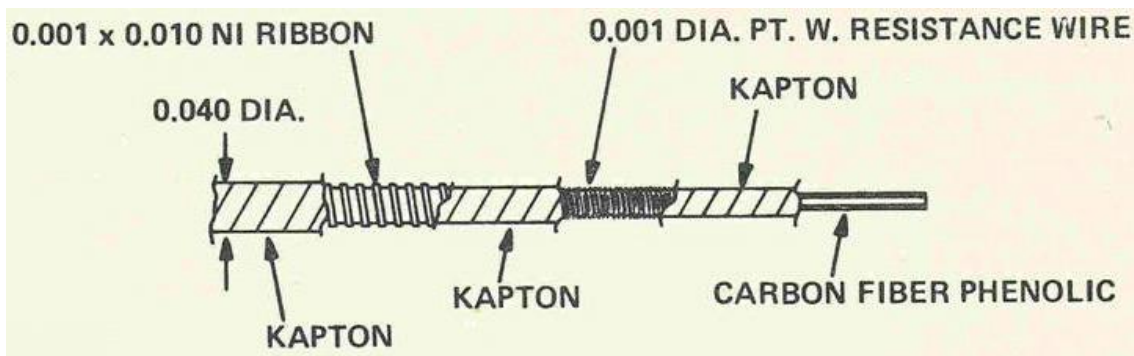


Figure 6: Schematics of Arad sensor. Each ARAD device consists of a narrow rod made of the ablator material itself (carbon fiber phenolic) wrapped with alternating layers of insulating tape (Kapton), Platinum-Tungsten wire, another Kapton layer, and Nickel ribbon [25].

² Facility to create representative of real hypersonic environments experienced in flight, in order to understand the TPS materials response to hot gas flow environment.

The ARAD sensors had multiple failures on the Galileo mission due to unknown reasons [3], but it is suspected that there was a low signal to noise ratio contributing to those failures. Another possible explanation for those failures is electrostatic discharging interference with the measurement.

3.2. HEAT

The Hollow aErothermal Ablation Temperature³ detector (HEAT sensor) measures recession through the corresponding change in resistance and requires an external constant current source excitation. Like ARAD, is an intrusive sensor because is necessary to drill holes in TPS to accommodate it. The HEAT sensor operating principle consists in using a hollow thin-film tube that chars at approximately 700 °C and because the char layer is electrically conductive it completes the electrical circuit between the two coils of wound wire, returning an electrical signal to indicate its length. The wire is made by platinum and is wrapped around a polyimide tube (See Figure 7). A core of the acreage TPS is inserted into the HEAT to reduce the sensor's disturbance to the local material.

The HEAT sensor was developed to overcome the shortcomings of the ARAD sensor package and was applied on MSL Entry, Descent and Landing Instrumentation (MEDLI) that flew on Mars Science Laboratory (MSL), landed on Mars on August 2012.

³ In some literature the acronym HEAT stands for Hollow aErothermal Ablation Tracking.

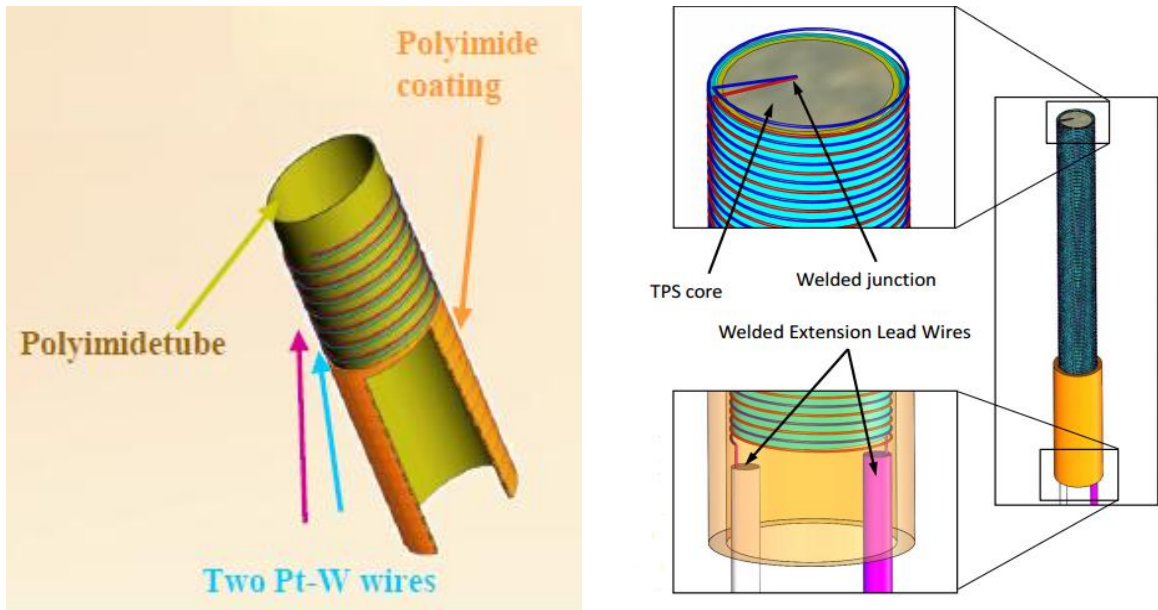


Figure 7: Heat Sensor. a) materials [26], b) schematics [27].



Chapter 4

The TPIP Project

4.1. Thermal Protection system sensor based on Impedance Probe (TPIP)

This project relates to an ablation sensor for spacecraft's thermal protection systems encountering very high temperatures during atmospheric re-entry. The major difference between available sensors and TPIP is that the others are intrusive. This project aims to create a non-intrusive electrical sensor to provide real time measurements of TPS surface recession of entry and re-entry spacecraft. It is based on Mutual Impedance Probe (MIP) used to measure the dielectric properties of the medium, and to infer TPS ablation in real time, with a minimum resolution of 0.5 mm for a shield thickness of 20 mm.

4.2. System Architecture

The architecture of the TPIP sensor comprises analogue, digital, and software modules (See Figure 8). The selected working frequencies for the analogue module are in ELF-VLF range. The waveform and associated modified signals are injected in the medium through a pair of transmitters, forming an electric dipole. The digital module includes the data acquisition system. The software module is responsible for signal processing, and data analysis and transmission, although it can also be done externally. The basic numerical algorithm used to assist with data analysis was the traditional Fast Fourier Transform (FFT), along with averaging techniques. Unlike FFT, sine-fitting algorithms

are immune to spectral leakage and noise since they act as very narrow band pass filters, tuning only the sine frequency and disregarding any other disturbances, this can be an future improvement in data analysis. For the Mutual Impedance technique, where both transmitting and receiving signals can be measured, one can use a seven-parameter sine-fitting algorithm, which computes the amplitude, phase, and DC component of the two signals as well as the common frequency. The differential signal is measured in the two receivers (Rx1 and Rx2) and a high-pass filter is included to remove the DC and quasi-static components and, consequently, improve sensor performance.

Noise induced by power lines is mitigated by decoupling capacitors placed as close as possible to the integrated circuits to minimize interference and crosstalk. The system uses coaxial and triaxial cabling to carry signals from the receivers and to the transmitters, respectively.

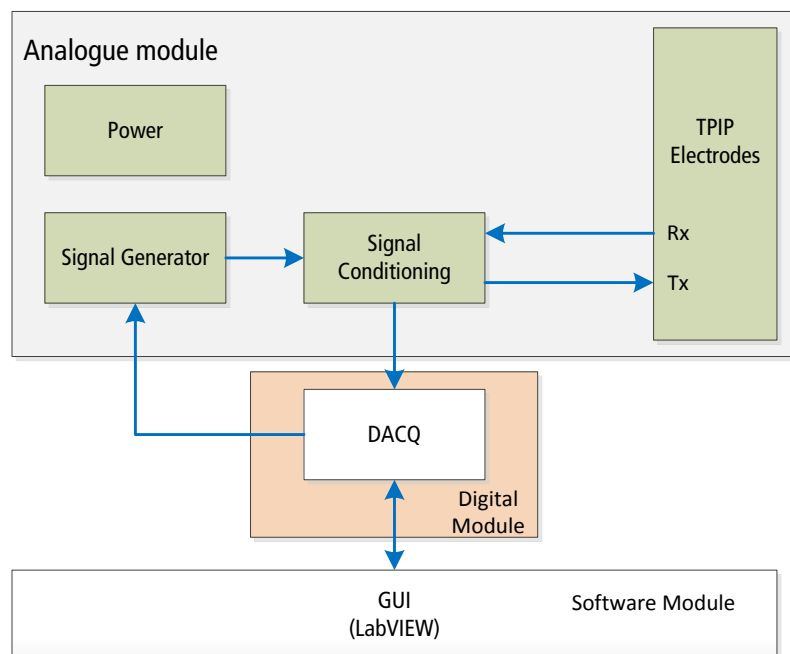


Figure 8: TPIP system architecture.

4.3. Mutual Impedance Probe

Impedance is an important parameter used to characterize electronic circuits, components, and materials used to make components. To determine the impedance, we need to measure at least two values since impedance is a complex quantity [16].

$$Z = \frac{V}{I} \quad (1)$$

There are different methods for measuring impedances. The method of choice depends on the frequency range, the magnitude of the applied signal, the desired accuracy and also the simplicity of implementation [17]. The most standard approach to measure impedance consists in applying a single-frequency voltage or current to the interface (electrodes) and measuring the phase shift and amplitude of the resulting current at that frequency, using either an analog circuit or a FFT analysis of the response. This approach is known as Impedance Spectroscopy (IS), can usually measure impedances as a function of frequency in the ranges from about 1 mHz to 1 MHz [18].

The Mutual Impedance (MI) is a technique that belongs to the broad domain of IS but uses a swept-frequency technique to measure the complex permittivity of a medium, which is related to the dissipation of energy within the medium. A periodic current of known shape, amplitude and appropriate frequency, e.g. a sinusoidal or square signal, is injected between two transmitting electrodes, known as Tx1 and Tx2, and induces a voltage difference between two receiving electrodes, Rx1 and Rx2, shown in Figure 9.

The impedance of the medium is supposed to be independent of the amplitude of the applied signal [18]. The sensor sensitivity is expected to be optimal when the material thickness is commensurate with spacing between transmitters and receivers [21].

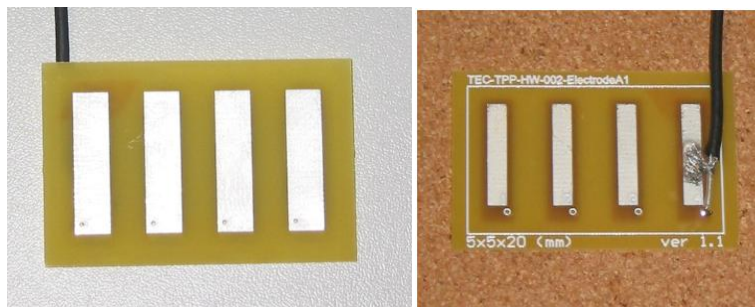


Figure 9: Electrodes assembly [1] a) Electrodes view b) Shielding view.

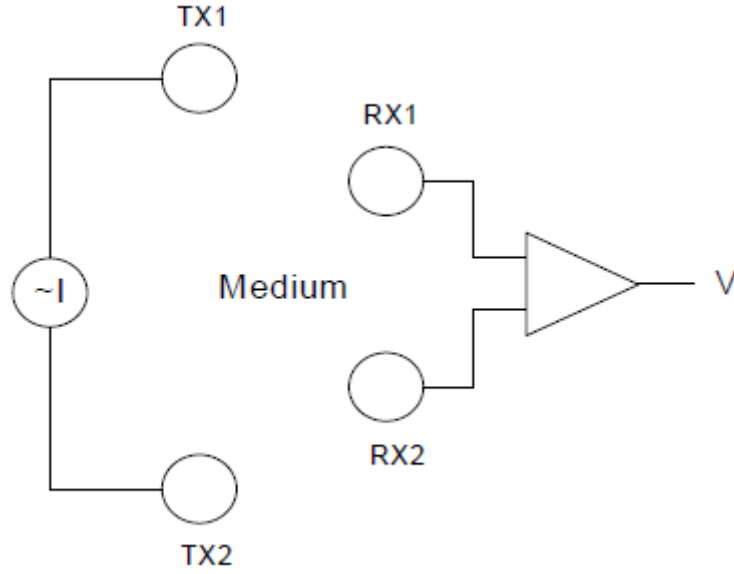


Figure 10: Principle of Mutual Impedance measurement [29].

The Mutual Impedance Probe (MIP) is an instrument that implements the MI technique and requires 4 electrodes (See Figure 10). A sinusoidal current of constant amplitude with a known frequency is injected between two transmitting electrodes (Tx1 and Tx2) inducing a voltage, V , between two receivers (Rx1 and Rx2) [19]. The ratio V/I , equation (1), is the mutual impedance of the probe. This requires a periodic signal that is used to drive the two transmitting electrodes. If the amplitude and phase of the signal are (A_0, φ_0) in a vacuum or other reference medium, and (A, φ) in given environment, the conductivity, σ , and relative permittivity, ϵ , of the medium are [20]:

$$\sigma = \frac{A_0}{A} \omega \epsilon_0 \sin(\varphi - \varphi_0) \quad (2)$$

$$\epsilon = \frac{A_0}{A} \cos(\varphi - \varphi_0) \quad (3)$$

where ω is the angular frequency of the stimuli and ϵ_0 the permittivity of the medium. Equations (2) and (3) are used to derive the dielectric properties of the medium and, indirectly, the TPS front surface recession. Since no galvanic contact is necessary between the sensor and the inspecting medium, the electrodes do not have to be embedded in the TPS. If we guarantee no air between the electrodes and TPS rear surface, sensor sensitivity is maximized. This topic will be discussed more in detail in next sections.

The relative sensor dielectric constant is given by:

$$\varepsilon = \varepsilon_r - i\varepsilon_i = \varepsilon_r - i \frac{\sigma}{\omega\varepsilon_0} \quad (4)$$

where ε_r and ε_i correspond to real and imaginary parts of the dielectric constant. The optimal response of the MIP is obtained when the imaginary part equals the real part, yielding to:

$$\varepsilon_r = \frac{\sigma}{\omega\varepsilon_0} \Leftrightarrow f = \frac{\sigma}{2\pi \cdot \varepsilon_0 \cdot \varepsilon_r} \quad (5)$$

In order to estimate the optimal stimuli frequency we need to assume $\varepsilon_r \sim 3$ and $10^{-9} \text{ Sm}^{-1} < \sigma < 10^{-7} \text{ Sm}^{-1}$ for a P50 medium (Figure 11), obtaining:

The range of optimal frequencies is therefore,

$$18 \text{ Hz} < f < 1.8 \text{ kHz} \quad (6)$$



Figure 11: P50 sheets from Amorim Cork Composites.

Preliminary dielectric characterization of the mentioned P50 (See Annex 1) was conducted by Professors Carmo Lança and Eugen Neagu, at Universidade Nova de Lisboa. The electrical conductivity measurements were performed with a relative humidity of 37% at 298 K, and the obtained results vary between 1E-9 and 1E-7 S/m [31].

P50 cork composite particles are the same particles used by EADS - Astrium for manufacturing the Norcoat-Liège composite used in thermal protection, and TPS for NASA launchers. The other material used to validate the system is Calcarb® from Mersen (See Annex 2) which has similar properties of new carbon based TPS.

4.4. Electrodes Integration

The electrodes mentioned above can be integrated on the internal surface of the TPS and measure the ablation occurring on the external surface of the shield, as shown in Figure 12.

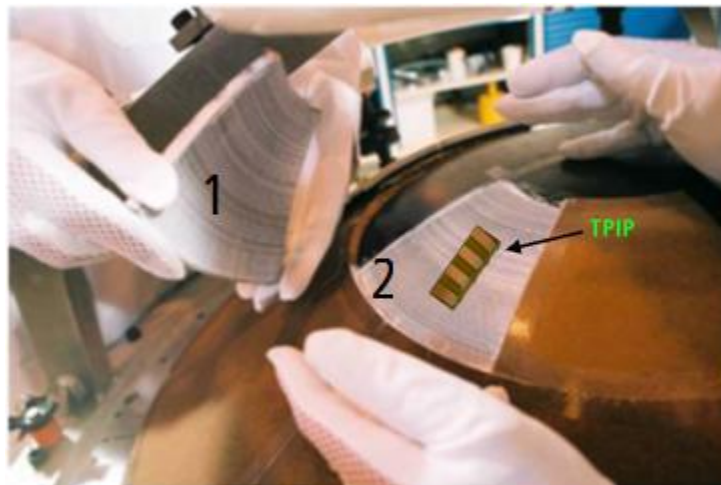


Figure 12: 1 - Ablative TPS layer; 2 - Internal layer. Adapted from [23]

To assess the most suitable integration solutions, we considered various alternative solutions, in particular:

1. Machining the TPS

In this solution it is necessary to machine the TPS surface to assemble the electrode inside a hole, keeping the surface flat, as shown in Figure 13.



Figure 13: Integration of the electrodes in the internal surface of TPS. In black is shown the wire used for the signals transmission between the electrodes and the data acquisition unit.

A small hole is needed to ensure the connection between the electrodes and the coaxial cable. One big problem of this solution is the fact that the volume of the layer is changed by the drilled hole and this has implications in the TPS properties. The solution for the problem mentioned above is to integrate the sensor without machining the TPS but the thickness of the electrodes can be an issue.

2. Flexible or rigid PCB glued to the TPS

This solution consists in gluing the electrodes directly on the ablative interior surface of the TPS. Using glue the air between the electrode and the surface is eliminated, the glue must be a special one that resists high temperatures and with a low electrical conductivity because otherwise a “short-circuit” can occur. The PCB can be rigid or flexible, depending on the integration zone, to ensure a perfect contact between the electrodes and the TPS structure.

3. Soldering

The soldering technique more adequate for this situation is the metal-ceramic brazing [22]. That is a process which parts are joined by a metal alloy of low melting pointing, without melting the base material.

4. Deposition

Physical vapor deposition is a set of processes used to deposit thin layers of material, typically in range of few nanometers to several micrometers in thickness. This process has three different phases: vaporization of the material; transportation of the vapor in vacuum to the substrate surface; and, condensation onto the surface thus generating a thin film. The Physical Vapor Deposition (PVD) can be done directly on the ablative TPS internal surface.

5. Using adhesive flexible copper foil electrodes

An uncomplicated alternative to make the electrode is to use adhesive copper foil. It is very easy to find in the market and is available with different tape thicknesses.

6. Using conductive paint to produce the electrodes directly on the TPS

The electrodes are obtained with conductive liquid paint, applied directly on the interior surface of the ablative TPS. To help to guarantee the required shape of the electrodes a mask is required, and the ink can be applied either with a jet or using a brush. This paint should be silver based because it is a good electrical conductor and is thermally stable.

The above solutions have been evaluated in detail, considering some aspects such as contact quality, sensor manufacturing, integration, robustness, weight, and cost. Regarding all the requirements (low mass, low power and non-intrusiveness) and issues we found that the silver paint electrodes are a very interesting solution. However, further tests need to be performed and for the TPIP prototype the electrodes are integrated in a PCB, as shown in Figure 9. The sensor sensitivity is higher using the PCB because silver paint electrodes are very noise susceptible.



Chapter 5

Test Results

A series of bench tests have been performed to validate the proposed solution and access if the proof of concept satisfies the goals and the project requirements, namely, in terms of suitability to perform non-invasive, real-time measurements of TPS thickness, and accuracy of such measurements. The results of the measurements were presented to the tester numerically and graphically by data processing module, using Labview®.

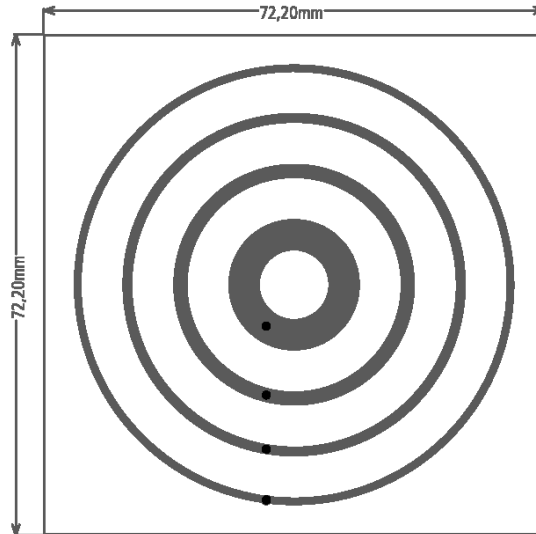
5.1. Electrodes Configuration Selection

Selection of the architecture of the electrodes must take into account several requirements. The size of the electrodes should depend of the sensor sensitivity and the sensor depth range, and should be similar to the separation between electrodes. Based in a theoretical assessment of the MIP concept, as well as on its optimization for measuring the TPS recession level, several electrode shapes and sizes were considered and tested (see Table 2). The tests are intended to validate the numerical model. To evaluate theoretically each configuration it was employed model with a finite element method to solve the generalized Poisson equation, from which one gets the potential distribution as function of medium properties. Each configuration has four electrodes, two are transmitters and two are receivers.

Configuration	Shape	Specifications
C1		Electrodes width: 5 mm Electrodes length: 20 mm Gap between electrodes: 5 mm
C2		Electrodes width: 10 mm Electrodes length: 20 mm Gap between electrodes: 10 mm
C3		Electrodes width: 15 mm Electrodes length: 20 mm Gap between electrodes: 15 mm
C4		Electrodes width: 10 mm Electrodes length: 50 mm Gap between electrodes: 10 mm

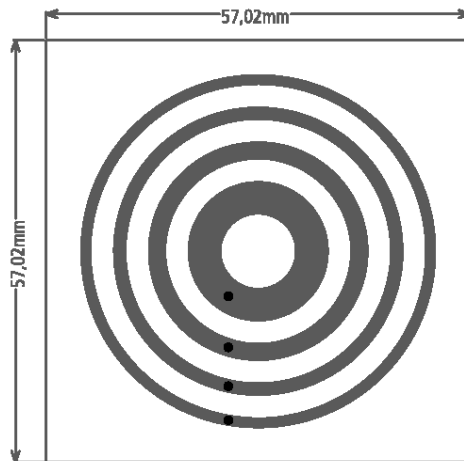
(Continues)

C5



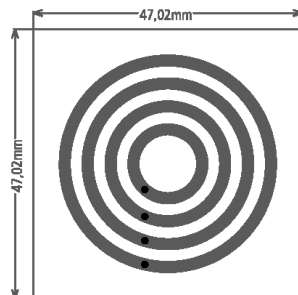
Most inner electrode radius: 5 mm
Electrodes area: 200 mm^2
Gap between electrodes: 6 mm

C6



Inner electrode radius: 5 mm
Electrodes area: 200 mm^2
Gap between electrodes: 3 mm

C7



Inner electrode radius: 5 mm
Gap between electrodes: 2 mm
Electrodes width: 2 mm

(Continues)

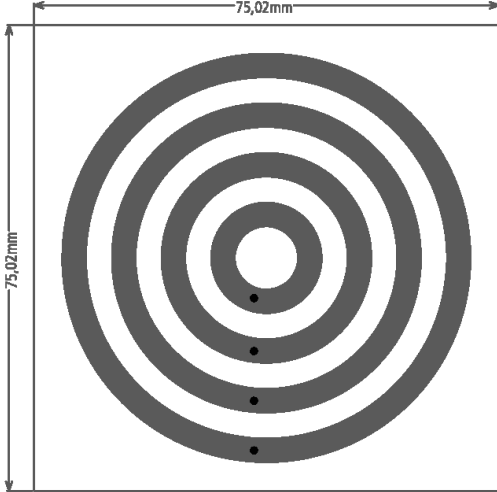
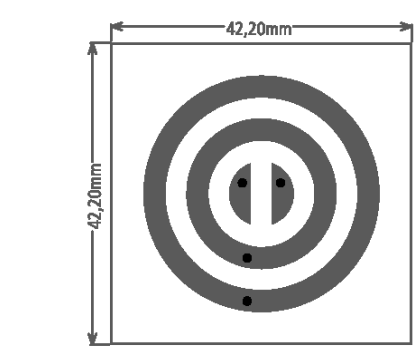
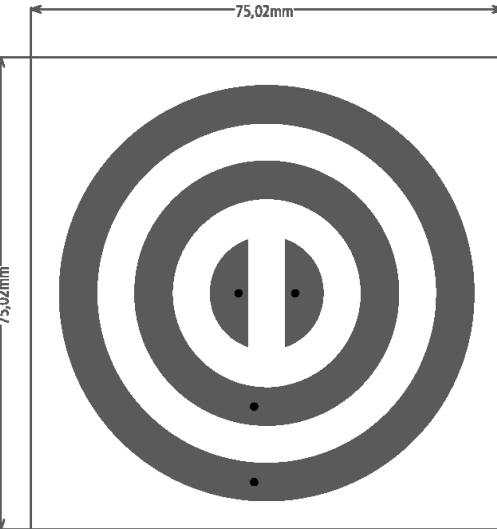
<p>C8</p>		<p>Inner electrode radius: 5 mm Gap between electrodes: 4 mm Electrodes width: 4 mm</p>
<p>C9</p>		<p>Dipole external diameter: 9 mm Dipole strip cut-out: 3 mm Gap between electrodes: 4 mm Electrodes width: 4 mm</p>
<p>C10</p>		<p>Dipole external diameter: 18 mm Dipole strip cut-out: 6 mm Gap between electrodes: 6 mm Electrodes width: 6 mm</p>

Table 2: Different electrode configurations [29].

5.2. Tested features

Tests have been performed some to validate the proposed concept, in particular the following aspects:

- Noise characterization at electronics level;
- Phase shift characterization at electronics level;
- Reference measurement of conductivity and permittivity;
- Characterization of all electrode configurations;
- Full characterization of the best electrode configurations;
- Environmental testing;
- Sensor behavior to the P50 pyrolyzation;
- Calcarb® testing;
- Characterization of silver painted electrodes using configuration 4;

The author was responsible for the preparation of test procedures and for testing the sensor, performing test 1 to 6 and test 12. The data from the other tests were provided by other members of the team and can be found in project final report [29]. The information about the other tests are present in this work because are important to understand some theoretical approaches. Particularly, pyrolysis test.

Some different tests have been performed to validate the proof of concept:

5.2.1. Test 1: Electronic noise characterization

This test intended to characterize the noise resultant from the signal conditioning board and the acquisition unit. The electrodes were replaced by well-known voltage dividers in order to minimize the effect of the electromagnetic field. With this test is possible to access the fluctuations of the system, namely if the amplitude and phase of the electrodes. The pass criterion was to achieve an error less than 0.1% at every applied

frequency. The system passed this test in most of all the frequencies, and was concluded that the electronics have a stable and accurate amplitude response (~0.07%).

5.2.2. Test 2: Phase shift characterization at electronics level

This test intended to characterize the phase shift introduced by the acquisition unit and the signal conditioning board. This kind of test is very important to ensure the accuracy of the measurements across the different materials. This was done by measuring its accuracy for various capacitances and the conclusion was that the precision of the sensor is the same for different materials. In terms of magnitude, the requirements have been met for every considered frequency. It was seen that as the frequency rises, the phase shift error decreases and it shows that phase measurements are less accurate than amplitude measurements.

5.2.3. Test 3: Measurements in Reference Materials

These measurements constitute a preliminary calibration of the TPIP system, using various materials with known dielectric properties (See Table 3). From this test on, the electrodes were connected to the respective Rx inputs and Tx outputs. To access the impact of the cables on the measurements, the test was made using two different cable lengths. When the size is bigger the attenuation rises, reducing the system sensitivity, because of cable capacitance.

Material	Permittivity [1]	Conductivity [$S m^{-1}$]
PTFE	2.1	5×10^{-13}
Polyamide/nylon	3.5	10^{-12}
ISOVAL	5.5	$10^{-12} - 10^{-10}$

Table 3: Dielectric properties of tested materials.

It can be concluded that the main goal of the test, which is measuring the amplitude and phase shift errors, was successfully archived because the results were similar for each tested material (polyamide, PTFE and ISOVAL®). The results are shown in Table 4. It was also acquired data measuring data of air to calibrate the sensor.

Material		Amplitude [dB]	Phase [°]
PTFE	Average	-23.2186	352.7957
	Standard deviation	0.0064	0.0180
Polyamide/nylon	Average	-13.9802	352.7738
	Standard deviation	0.0040	0.0173
ISOVAL	Average	-20.0252	355.3460
	Standard deviation	0.0035	0.0294
Air	Average	-24.6071	350.3421
	Standard deviation	0.0032	0.0279

Table 4: Calibration of TPIP sensor. Data acquired at the frequency of 1 kHz and using cables of 38 cm of length.

5.2.4. Test 4: Characterization of All Electrode Configurations

This test case was intended to select the most suitable configuration for thickness measurements, regarding in particular the shape and size of all 10 electrode configurations (linear and circular architectures), previously selected (See Table 2). Additionally these measurements can be used to validate the finite element results. For this test we made various measurements of the amplitude and phase for P50 thickness in the range from 5 to 20 mm, calculating the mean value and standard deviation of the measured signal. The test assembly is shown in Figure 14. From this test on, the electrodes are attached to the P50 samples by means of epoxy glue that possesses good dielectric properties.

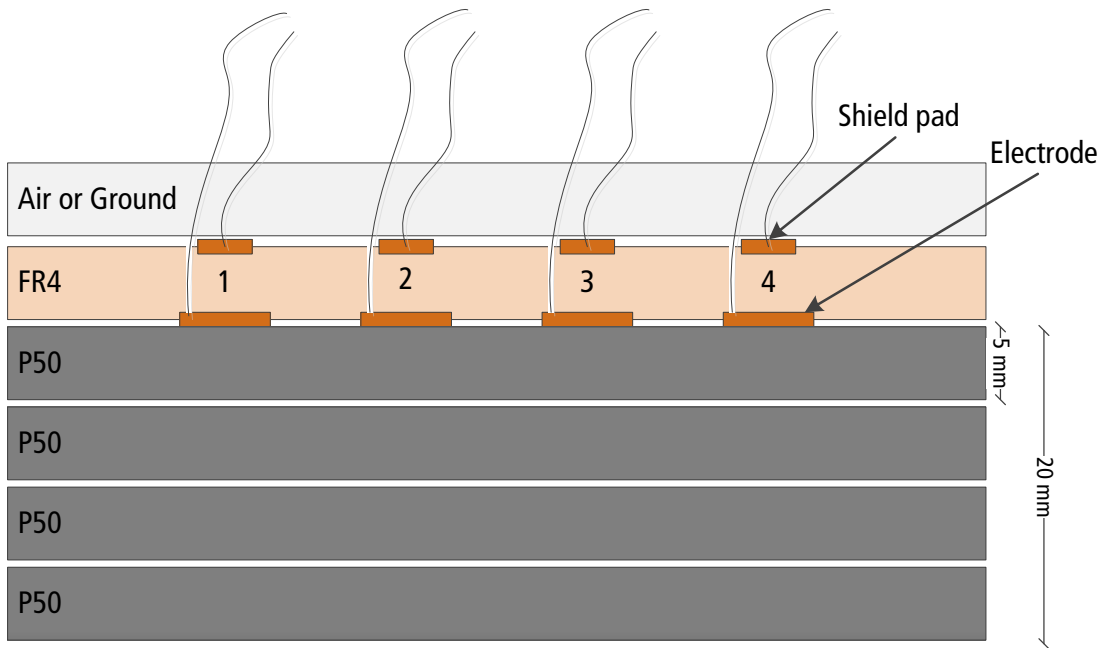


Figure 14: Characterization of all 10 different electrode configurations measuring P50 samples. FR4 is an epoxy based composite present on printed circuit boards (PCB) and is where the electrodes are integrated.

Larger variation in amplitude or phase with thickness means higher sensitivity. However it is necessary to verify if the error bar is acceptable. This means a choice is made based upon the slope of the curve and associated errors. Monotony is just considered as tiebreaker. Plots in Figure 15, Figure 19, Figure 17, Figure 18 and Figure 19 show the three best results of the amplitude and phase for each frequency among the 10 configurations. From top to bottom, the considered frequencies are: 10 and 200 Hz as well as 1, 10, and 100 kHz. For the sake of visualization, all the data is normalized against the values for a thickness of 5 mm.

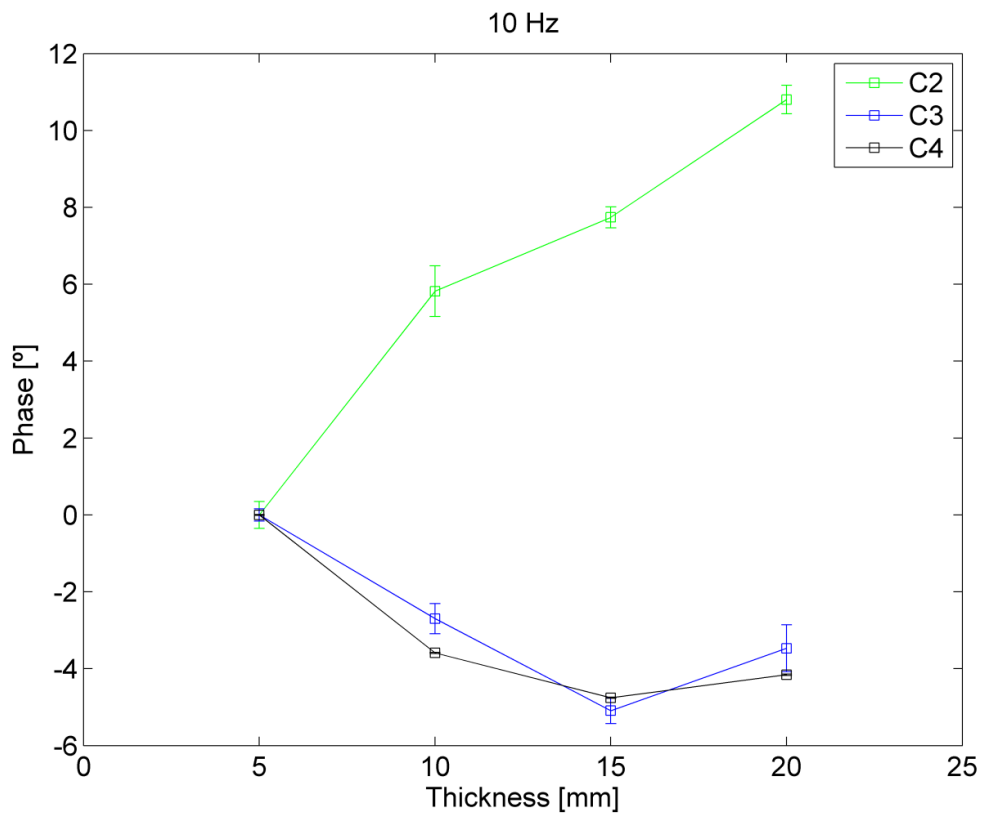
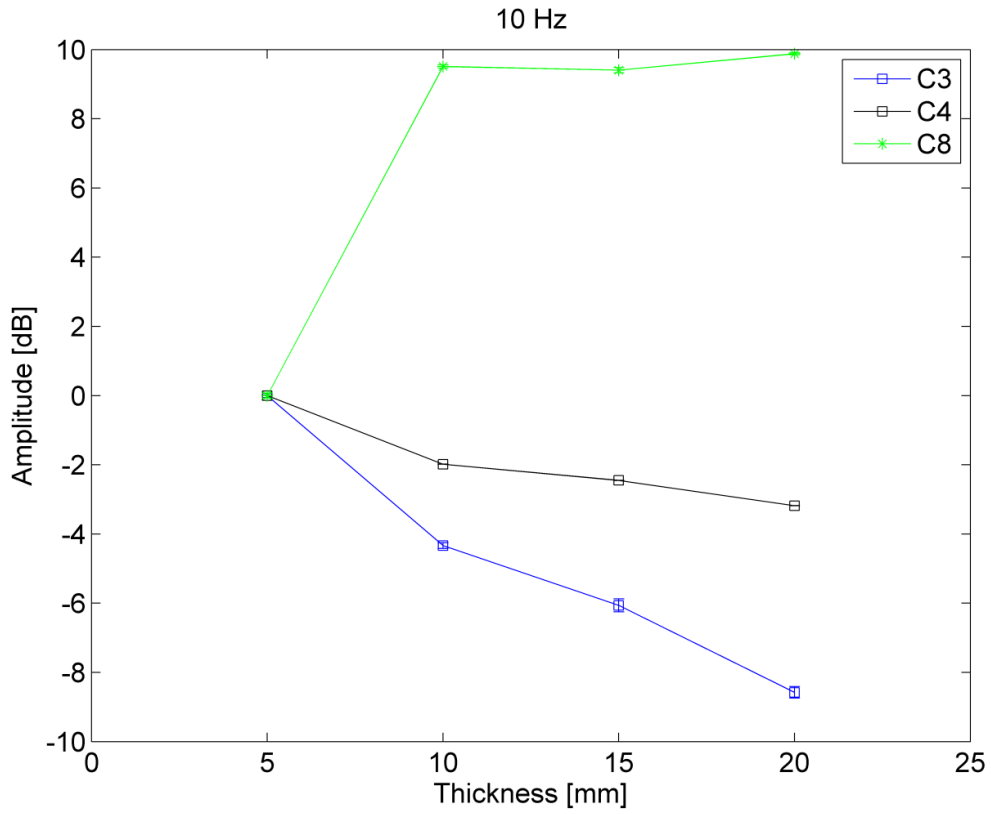


Figure 15: Mean and standard deviation of the amplitude and phase as a function of thickness at 10 Hz [29].

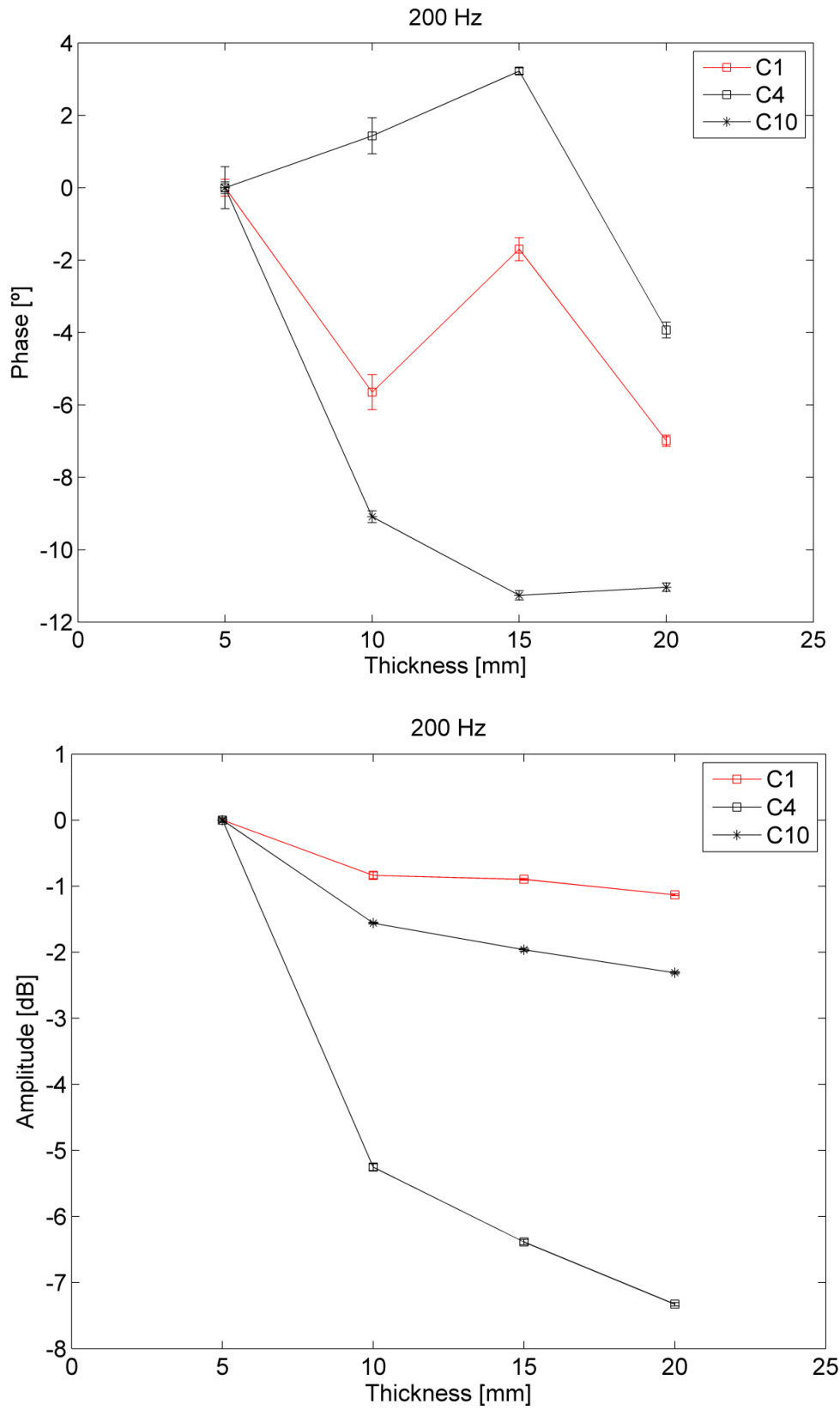


Figure 16: Mean and standard deviation of the amplitude and phase as a function of thickness at 200 Hz [29].

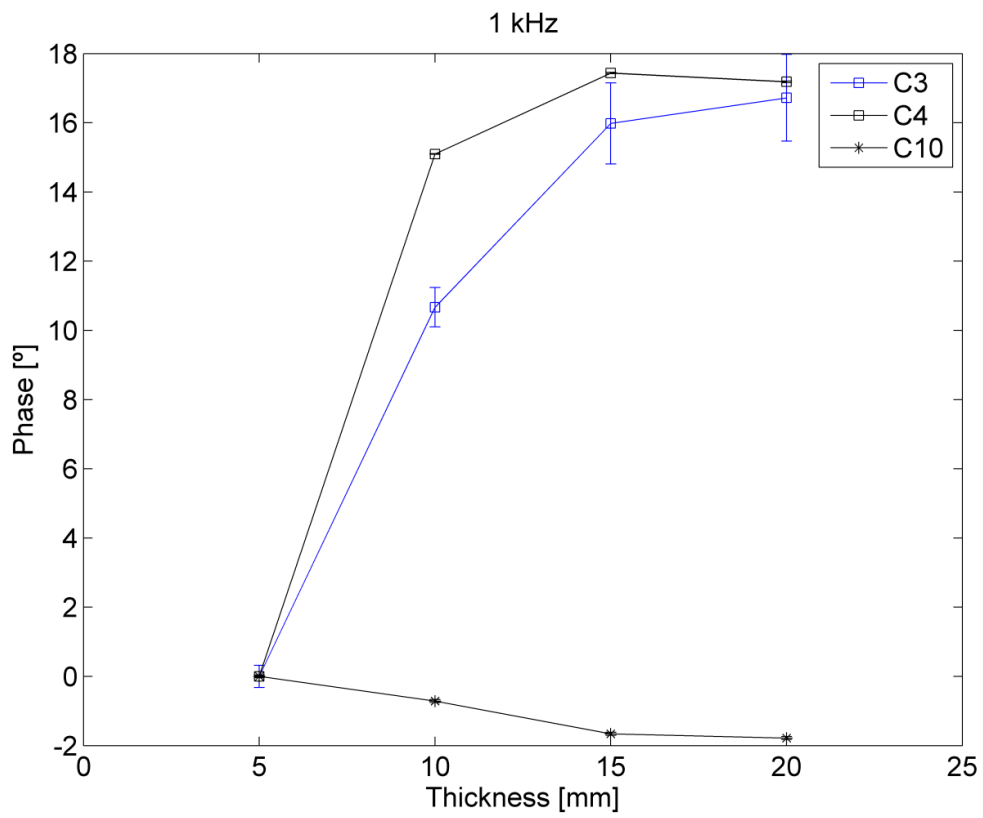
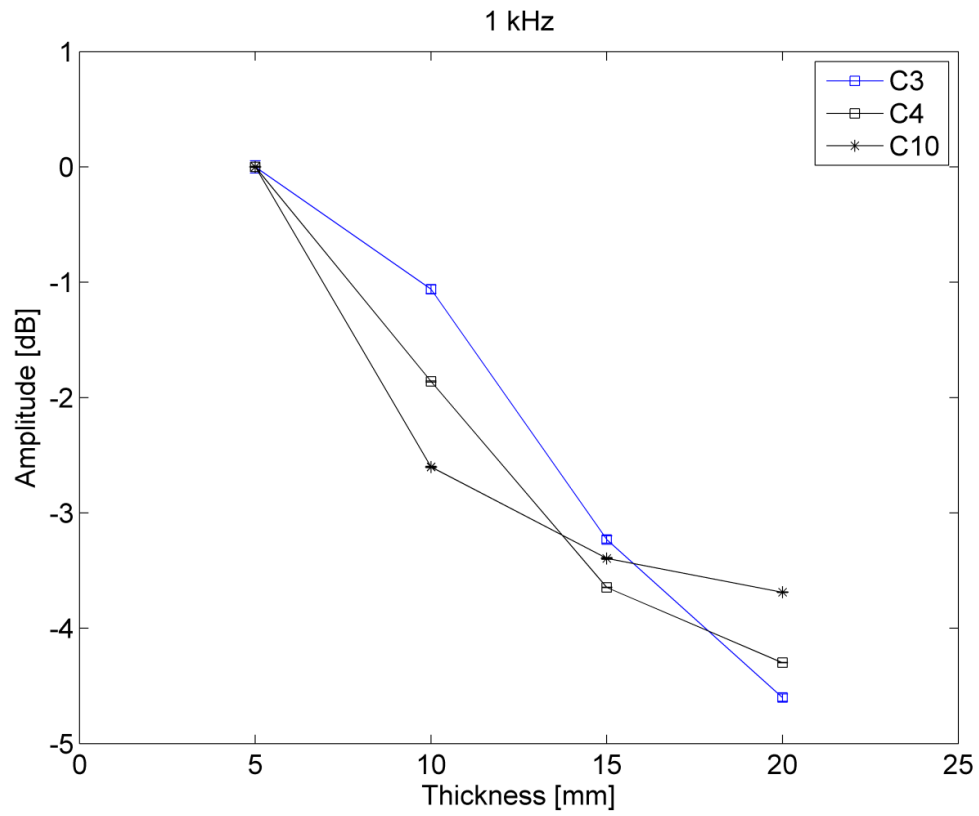


Figure 17: Mean and standard deviation of the amplitude and phase as a function of thickness at 1kHz [29].

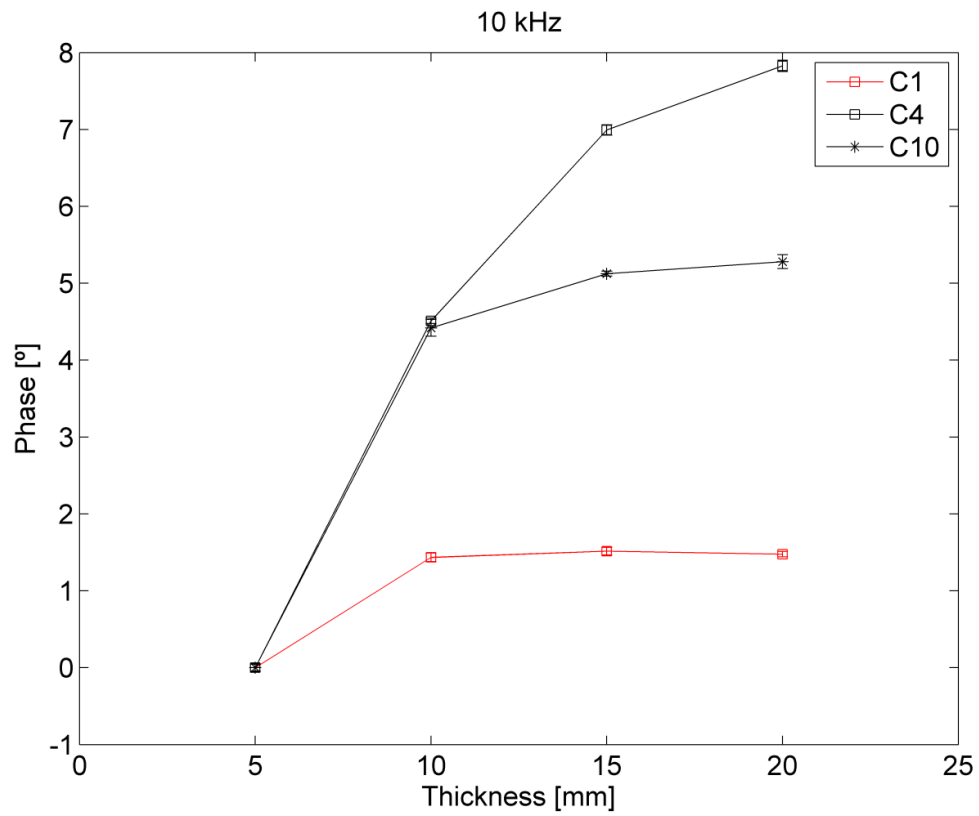
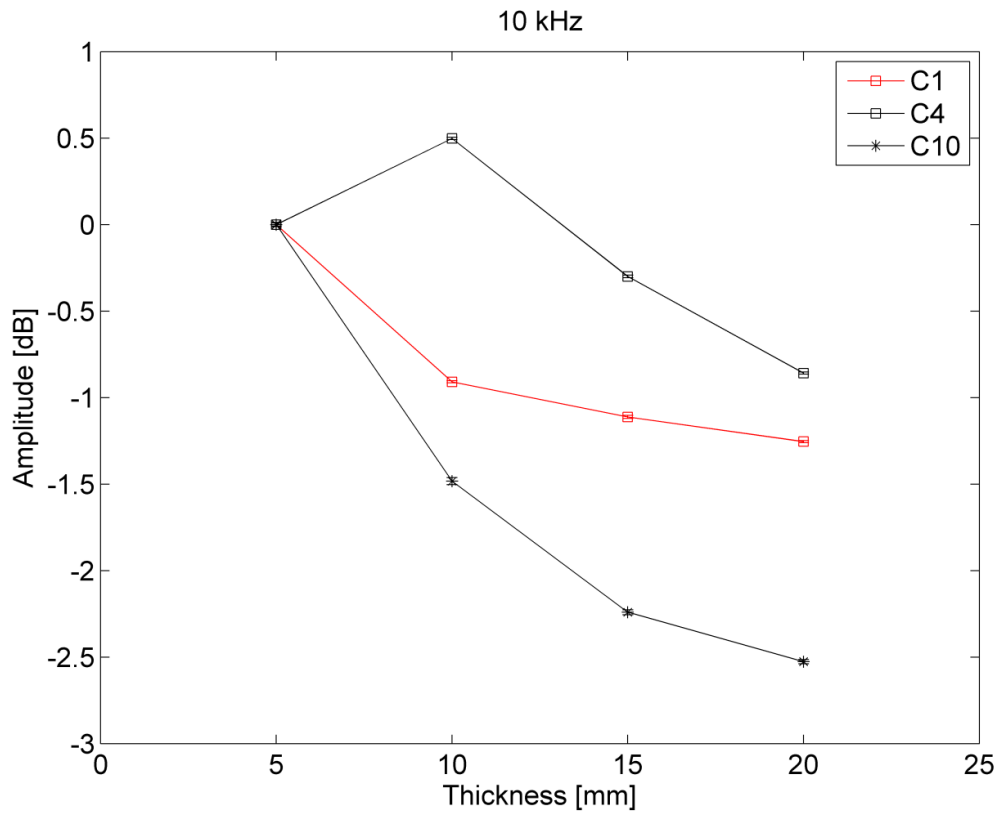


Figure 18: Mean and standard deviation of the amplitude and phase as a function of thickness at 10 kHz [29].

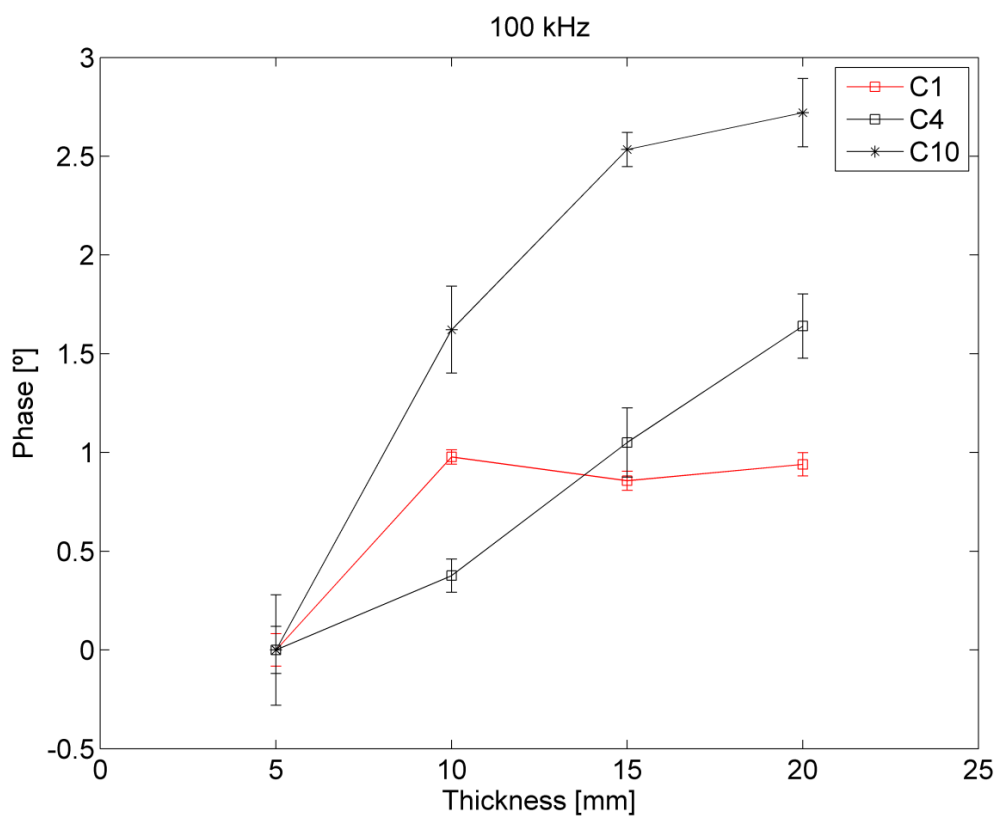
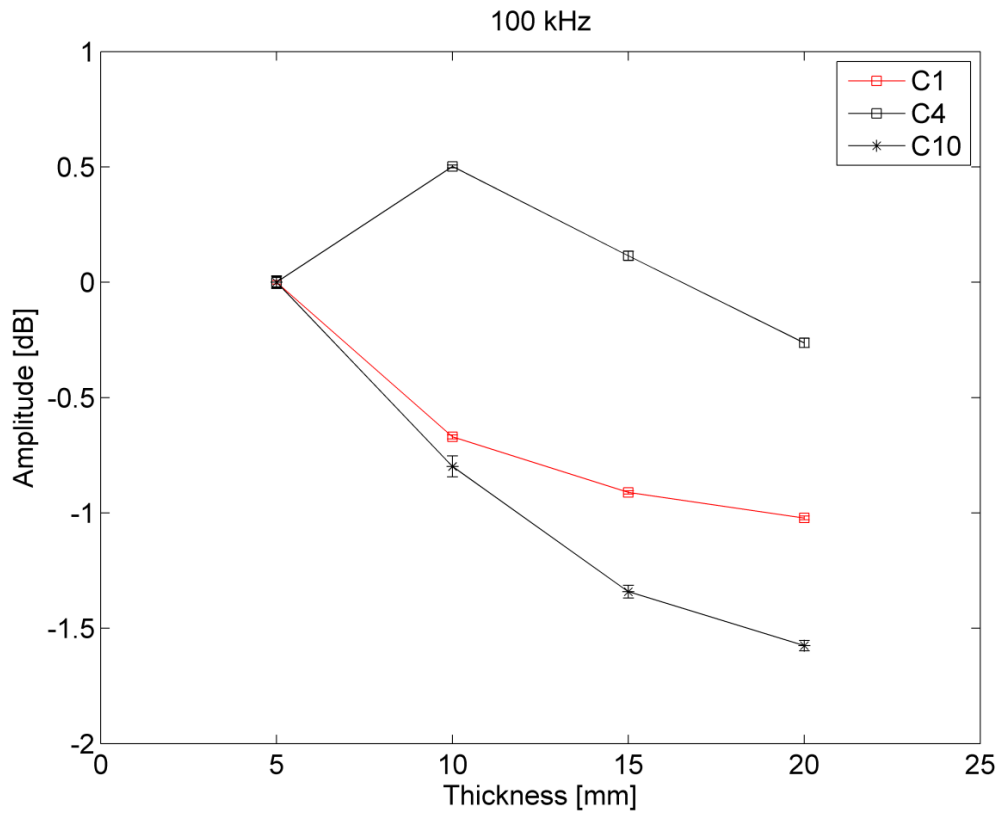


Figure 19: Mean and standard deviation of the amplitude and phase as a function of thickness at 100 kHz [29].

Table 5 shows how often each configuration appears among the best three configurations for each different injected frequency. The configurations that not appear among the best three are not present in the table.

Configuration	x_i
C1	6
C2	1
C3	4
C4	10
C8	1
C10	8

Table 5: Number of time a configuration appears among the best configurations for each frequency.

In order to support the decision of what configurations are best, a trade-off was made. The most relevant results include:

- The best square configuration is C4 because it is the one that has the highest variation over the P50 thickness range;
- The best circular configuration is C10, for the same reason mentioned above;
- Configuration C1 has been selected because it could be interesting to measure thin layers since is a small size electrode configuration, with a short spacing among them.

5.2.5. Test 5: Full Characterization of the Best Electrode Configurations

This test is a repetition of test case 4 but just for the best configurations, made with smaller thickness steps in order to calculate the expected accuracy of the measurements, namely the mean and standard deviation. The results from this are also useful to validate the numerical model used in the simulations.

It was possible to conclude that the most suitable configurations are configuration 1 (small electrodes) for thin layers, and configuration 4 (large electrodes) is more accurate for layers of at least 20 mm. By the increment of smaller thickness steps it was possible to access that the homogeneity of the medium has a reasonable influence on the measurements of the sensor, in other words, it is different to measure five sheets of cork of 1 mm thick or measure a layer composed by just one sheet of 5 mm.

5.2.6. Test 6: Environmental Tests – DC electric field

The goal of this test case was to assess the influence of an external DC electric field on the TPIP measurements. A known electric field is applied when the thickness measurements are performed. These results are then compared with similar measurements without DC field. For this purpose, two aluminium sheets separated by 100 mm were mounted in the proximity of the TPIP sensor. The bottom layer was grounded, and that on top was biased to 50 V, creating an electric field of 500 V m^{-1} , as represented in Figure 20.

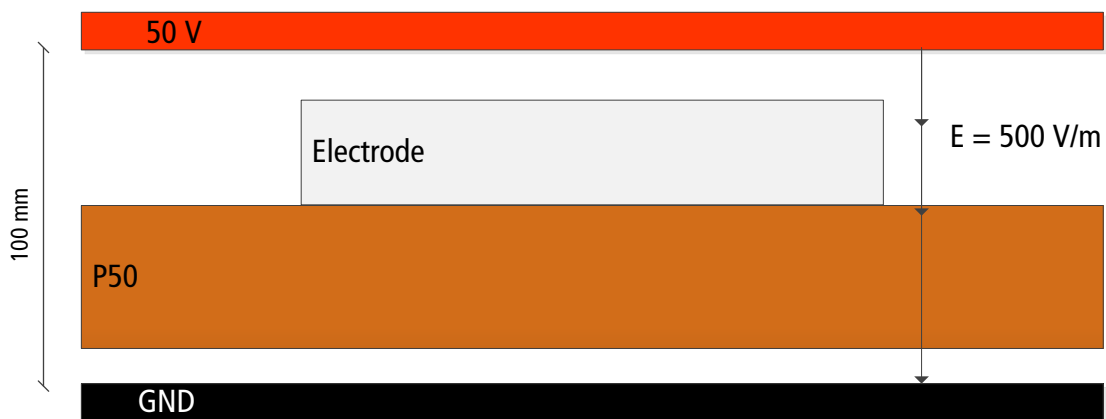


Figure 20: Electric field representation.

To verify the influence of an electric field on the TPIP measurements, a test with the duration of approximately 270 seconds is performed, divided in two stages (without and with an electric field, respectively). The results for 1, 5 and 10 kHz are plotted in Figure 21.

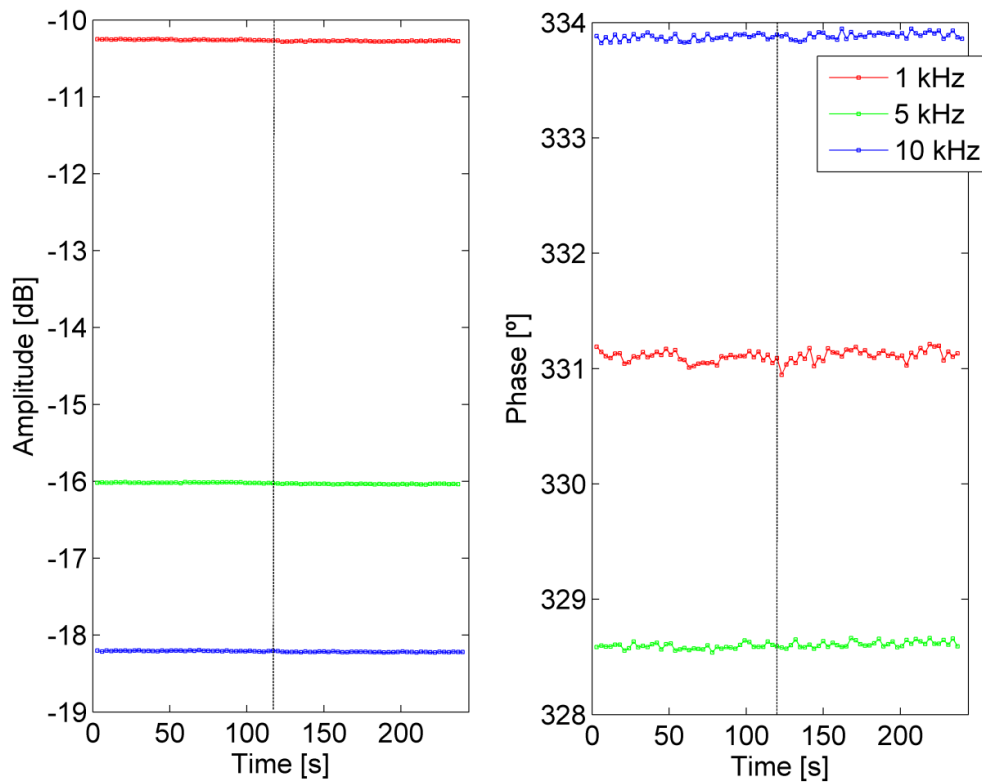


Figure 21: influence of DC electric field on TPIP measurements. The vertical dashed line identifies when the electric field is turned on [29].

As the variations with a 500 V m^{-1} field are minor, the direct effect of electric fields can be disregarded for most space applications.

5.2.7. Test 7: Environmental Tests – DC magnetic field

The goal of this test case was to assess the influence of an external static magnetic field on the TPIP measurements. For this test we performed some measurements of the amplitude and phase with and without a known magnetic field produced by permanent magnets, and compare the results.

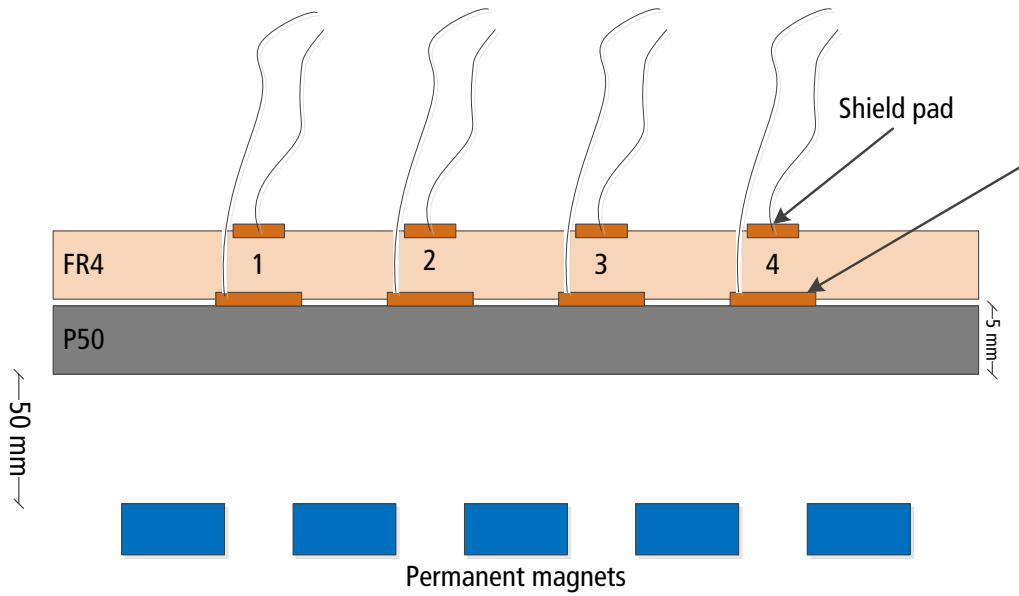


Figure 22: Magnetic field test assembly.

For the assembly shown on Figure 22, the magnetic field in vicinity of the electrodes is of the order of 10 mT. In order to verify the influence of a DC magnetic field on the TPIP measurements, a test with the duration of approximately 320 seconds was performed, divided in two stages (with and without a magnetic field). This test was similar to that for DC electric field. The results for frequencies of 1, 5 and 10 kHz and a distance from the magnets to TPIP of 5 cm are plotted in Figure 23.

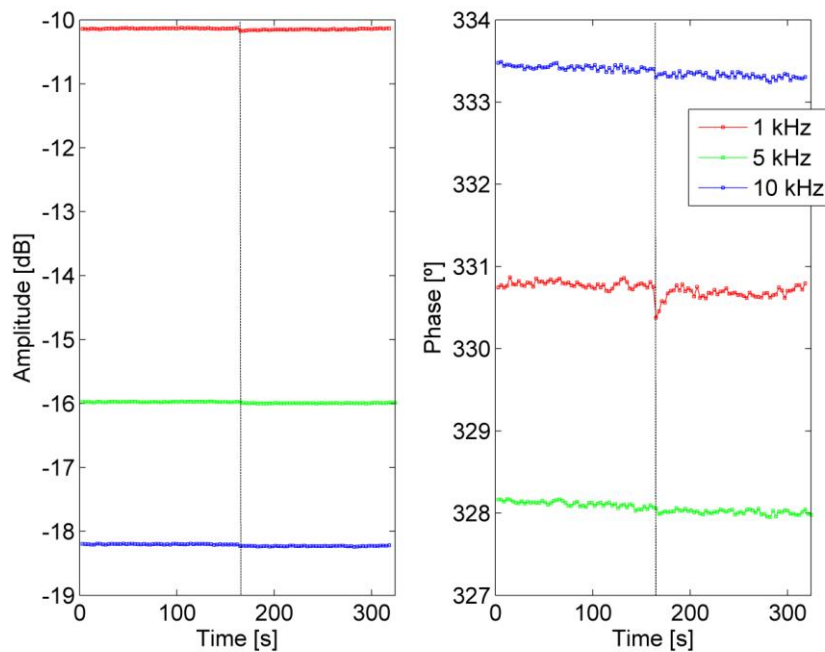


Figure 23: Influence of a DC magnetic field on TPIP measurements [29].

The influence of a DC magnetic field is not negligible for amplitude and phase measurements, as one can see an offset when the field is imposed. Moreover, the amplitude is more susceptible to the field than the phase, since a variation can be perceived farther from the electrodes. It was possible to observe that when the distance is reduced, the medium is more affected by the field, but at 5 cm distance we can only see the offset in the amplitude measurements.

The magnetic field has limited impact on this type of sensor. In fact, the value of the magnetic field on the Earth surface is about 50 μT while the applied field is approximately 10 mT. The field applied to the sensor is much stronger than what is expected to be found in space applications.

5.2.8. Test 8: Environmental Tests – equipotential surface

The goal of this test was to assess the influence of the plasma on the TPIP measurements. Plasma electrical properties are approximated by an equipotential surface made up of an aluminium sheet on the P50 layer. Again, the results obtained were compared with and without AC sheet. The test assembly is shown in Figure 24.

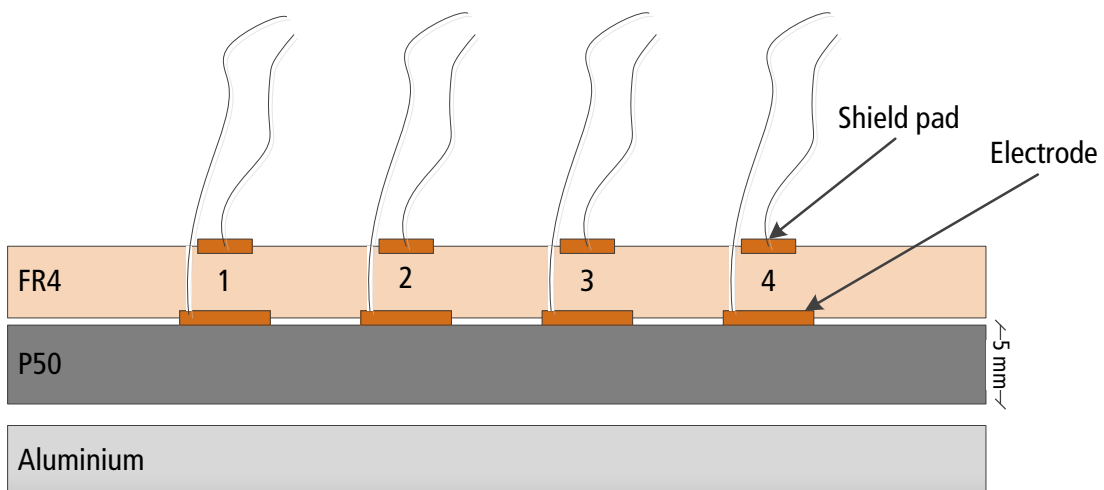


Figure 24: Equipotential test setup.

In theory, when an equipotential surface is placed over a layer of P50, the field lines are forced to redistribute themselves, so that the field satisfies the boundary conditions

given by the equipotential surface and the transmitting electrodes, affecting the way the field lines cross the receivers, leading to a reduction in the sensitivity of the sensor (see Figure 25).

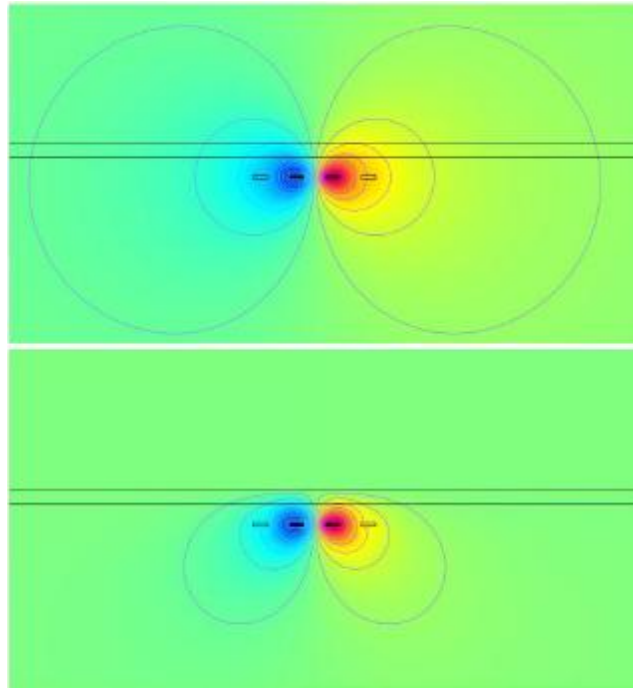


Figure 25: Electric field distribution with (bottom) and without (top) an equipotential surface [28].

As the equipotential surface moves away from the electrodes, it is expected that the electric field effect weakens. Figure 26 plots the amplitude and phase as a function of thickness for a normal layer of P50 compared to a layer of P50 with an equipotential surface above it.

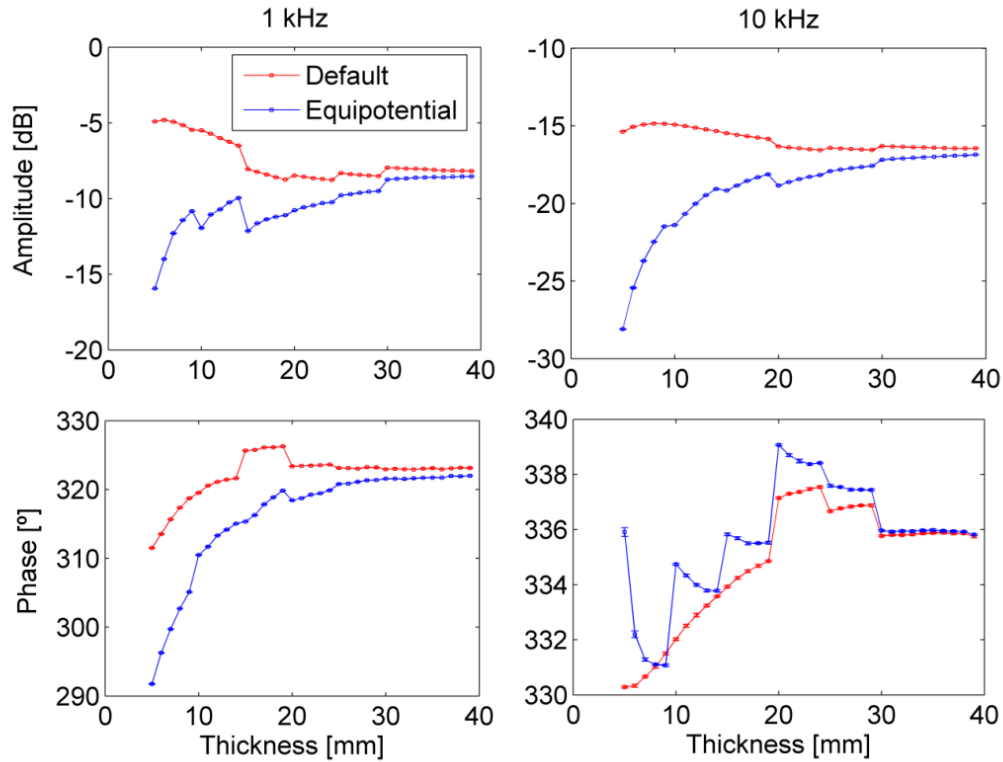


Figure 26: Amplitude and phase as function of thickness with and without equipotential surface [29].

The results confirm the behavior that was theoretically expected. It is possible to note the jumps resulting from the non-homogeneity of the medium (P50 cork). From observation of the plots of Figure 26, one can also see that the variation in amplitude and phase is not negligible when the layer is subjected to an equipotential surface. Therefore, the effect of creating plasma on the thermal protection system must be taken into account in the development and utilization of the sensor.

5.2.9. Test 9: Environmental Tests – thermal testing

The goal of this test case was to assess the influence of environment temperature on TPIP measurements. This test consists in performing some thickness measurements inside a thermal chamber, at different temperatures, and comparing the results with a similar test under normal conditions. Figure 27 shows the thermal chamber used in this test.



Figure 27: Thermal chamber test [29].

The cables held up a maximum temperature of 125°C, at which point the test was stopped. Figure 28 plots the amplitude and phase for all intervals from 50°C to 125°C.

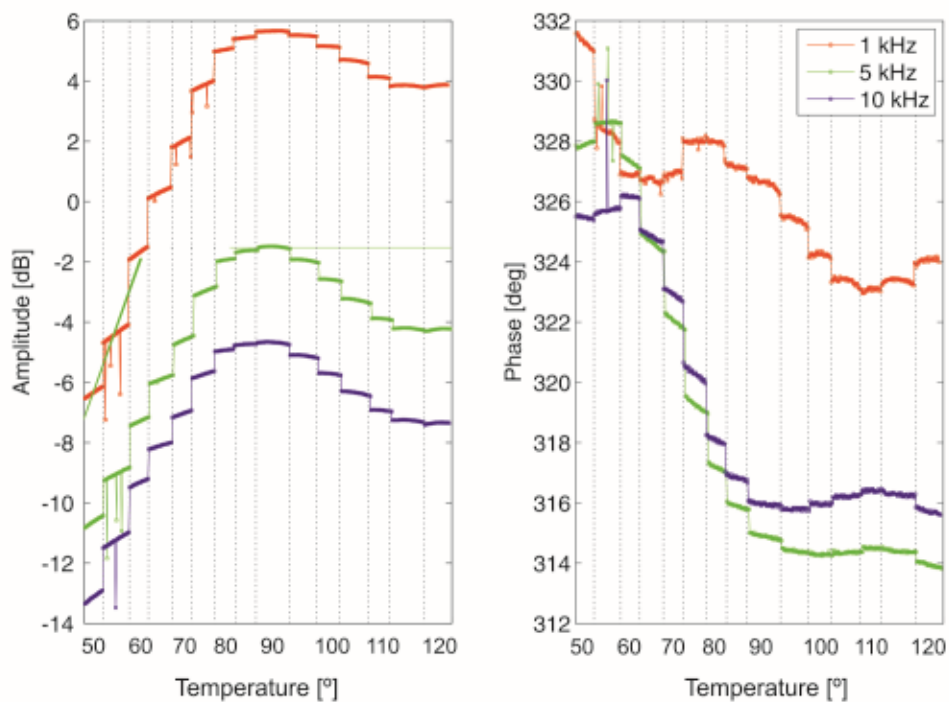


Figure 28: Influence of temperature on amplitude and phase measurements. Results for a P50 sheet of 5 mm thick [29].

As expected, the measurements vary with temperature. This variation can be related to polarization, i.e., the dielectric properties of the medium, the electrodes and cabling.

A comparison between measurements made with these materials provides useful insights to understand the significance of the thermal and electrical conductivities.

Corroborating our predictions from theoretical models, a large increase in electrical conductivity reduces sensor sensitivity. Therefore, the Rx gain must be increased to allow for sensitivity maximization to the expense of sensor noise increase. Evaluation of the impact of temperature in the Rx signal is thus necessary to obtain a reliable calibration of the sensor. In addition, these results are also important to rank effects of temperature in the electronics, cabling, and in the medium. To decouple the effects of temperature in the medium and the sensor, the electrodes and the thermal protection system must be separated by a material that possesses low thermal conductivity, low permittivity, and low electrical conductivity. If the TPS temperature indeed introduces a major perturbation in measurements, then careful data analysis is required to assess impact of heat in sensor performance.

5.2.10. Test 10: Test of sensor behavior of P50 pyrolyzation

This test case intended to evaluate how TPIP performs whenever the TPS is composed by intact and charred materials. In this test the pyrolyzation was achieved by means of a blowtorch. Figure 29 shows the pyrolyzation test assembly.



Figure 29: P50 burning [1].

In Figure 30 it is possible to identify 4 stages occurring in this test:

1. The acquisition has started but the torch is still not ignited and the amplitude remains constant;

2. The torch started to burn the P50 plate and the amplitude starts decreasing. This is the effect of both the equipotential surface in the plate and overall, the amplitude decreases almost 15 dB. The effect of the thickness decrease can be also responsible for the amplitude variation;
3. The torch continues to burn the P50 plate and the amplitude increases. This phase comprises the effect of the temperature increase (a variation of 40 dB is noticed);
4. The torch continues to burn the P50 plate and the amplitude saturates. At which point the test is stopped.

It is important to keep in mind that phase behaviour is quite different for different electrode configurations, in this case it was used the configuration 1.

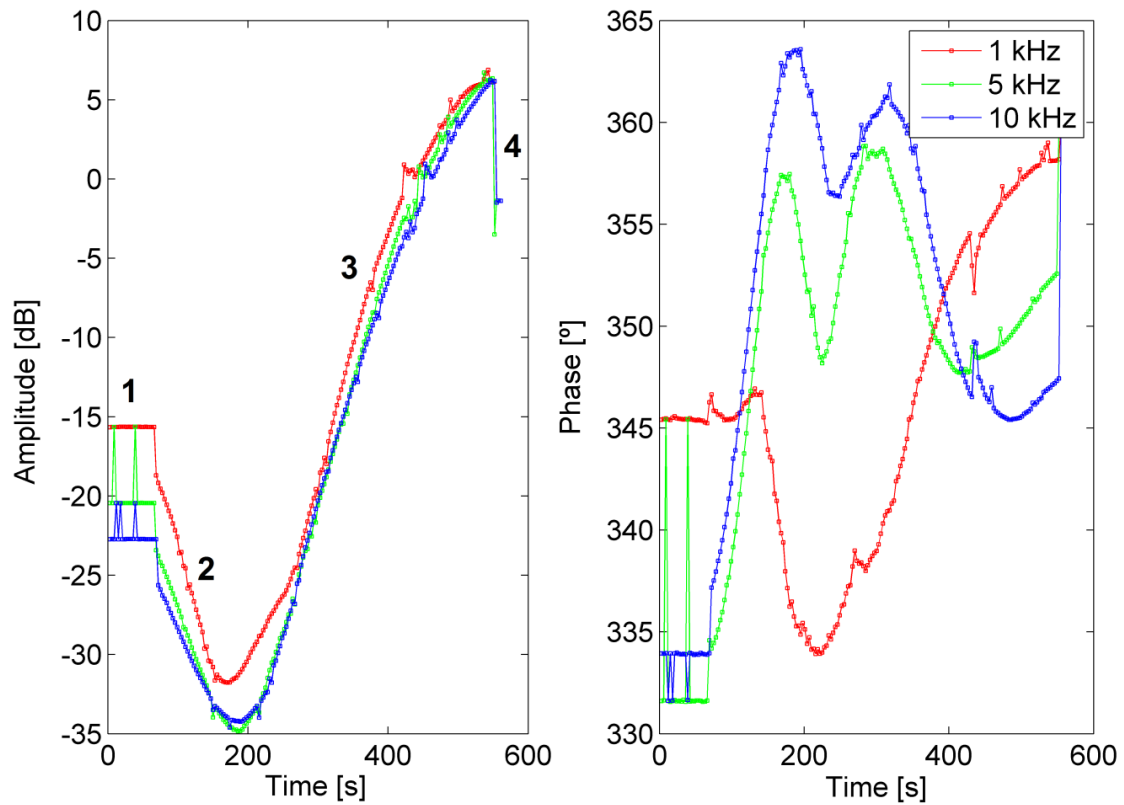


Figure 30: Influence of heat and pyrolyzation on TPIP measurements. P50 with thickness of 10 mm [29].

We conclude that the sensitivity of the TPIP is good enough to clearly identify the different stages that occur during the burning, as intended.

5.2.11. Test 11: Calcarb® Testing

This test case intended to characterize the TPIP measurement response of a material that allegedly is included in TPS composites.



Figure 31: Testing TPIP response to thickness increase with Calcarb® layers. Note that the sensor is attached to a P50 plate with 5 mm thick [1].

Two types of tests were considered: The first was a test to evaluate the sensor response to thickness variations, as discussed in 5.2.5 (test 5) using P50 layers, see test assembly on Figure 31; the second experiment describes Calcarb® pyrolization, similar to 5.2.10 (test 10).

From the left hand side of Figure 32, we can see that the amplitude measurements provide a resolution better than 0.7 mm for a 45 mm thick Calcarb® plate which is a very promising result for a material with such high electrical conductivity. Because of the high conductivity of the medium, phase measurements are much less relevant.

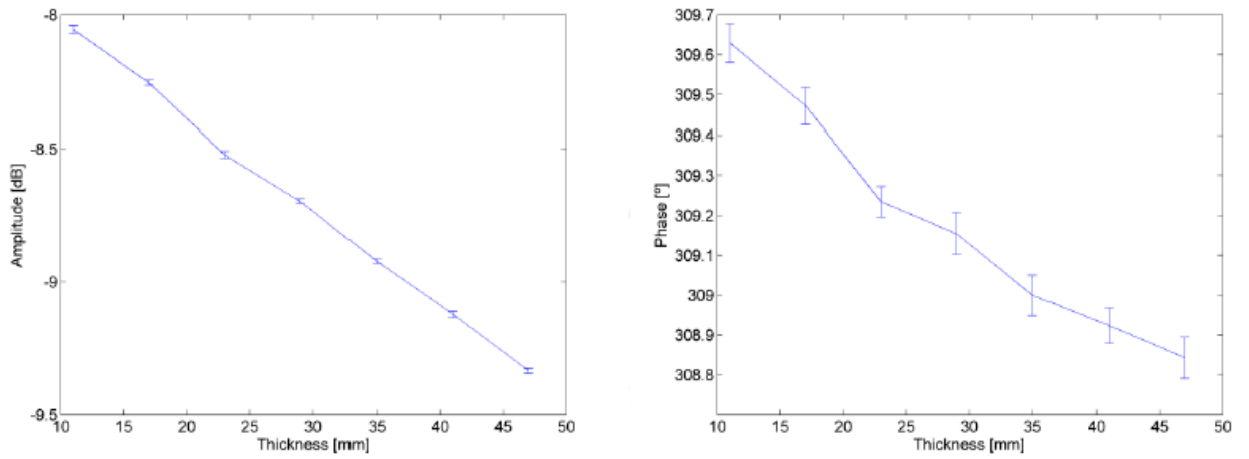


Figure 32: Amplitude and phase as a function of thickness at frequency of 1 kHz [29].



Figure 33: Calcarb burning [1].

As for the P50 pyrolysis test, it is important to analyze the main variables driving the variation of the amplitude and phase shift: plate thickness, temperature and plasma. We can see in Figure 34 the progress of the amplitude and phase during this experiment.

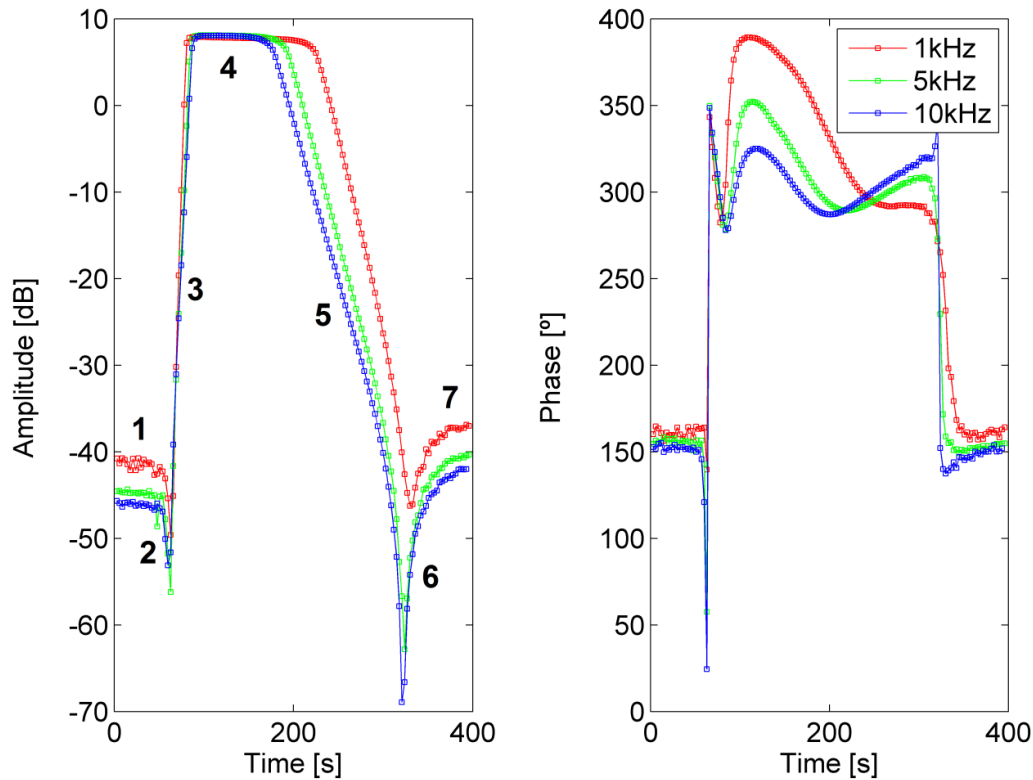


Figure 34: Influence of heat and pyrolyzation on TPIP measurements - Calcarb® with thickness of 18 mm [29].

It is possible to identify 7 main stages in this test (the first 4 are similar to those in P50 pyrolysis test that have been performed previously):

1. The acquisition has started but the torch is not ignited, thus the amplitude is constant (It starts at approximately -40 dB instead of -15 dB because the environment is now different);
2. The torch started to burn the P50 plate and the amplitude decreases. This phase primarily comprises the effect of the equipotential surface in the plate since the amplitude decreases almost 15 dB. The effect of thickness decrease can be also responsible for the amplitude decrease;
3. The torch continues to burn the P50 plate and the amplitude increases sharply. This phase comprises the effect of the temperature increase since a variation of 50 dB is noticed; this increase is sharp because the thermal conductivity of the plates is orders of magnitude higher than that of P50;
4. The torch continues to burn the P50 plate and the amplitude saturates. At this point the torch is stopped;
5. The temperature of the layer decreases and the amplitude also decreases;

6. A peak in the amplitude and phase signals is perceived. This peak is apparently not related to the processes discussed previously and we do not understand its origin;
7. The signals stabilize on the initial values when the initial temperature is reached.

The electrical and thermal conductivity of Calcarb® is very high when comparing to cork, a P50 of 5 mm thick plate was introduced. The sensor was attached to one side of P50 layer and pyrolyzation occurred above the Calcarb® plate. Figure 35 plots the response for this test.

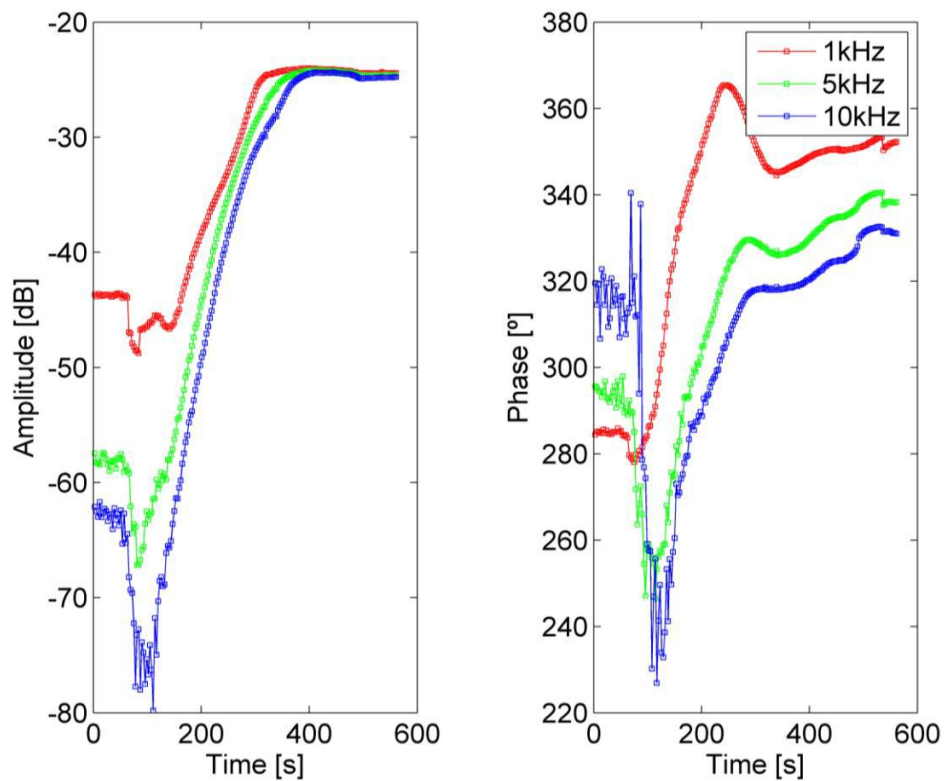


Figure 35: Influence of heat and pyrolyzation on TPIP measurements. P50 - 5 mm and Calcarb® - 18 mm [29].

Since cork is a worse thermal conductor than Calcarb®, it is possible to see a similar response to the previous test, with the effect of temperature on the electrodes spreading over a wider period. However, the test is stopped in stage 4, when the amplitude saturates.

5.2.12. Test 12: Characterization of silver paint electrodes

This test intended to evaluate an alternative method to create and assembly the electrodes painting them on the TPS surface.

In this test the electrodes were processed with conductive liquid paint, directly dried on the ablative TPS surface, as shown in Figure 36. The manufacturing process consists in laying down a mask on the TPS surface with the required shape of the electrodes, and then painting the electrodes with ink jet solutions or even a brush (it was used a brush). Ink application is very simple and some solutions are curable at room temperature. The used ink was PELCO® Colloidal Silver aqueous solution, which contains 60% of silver.

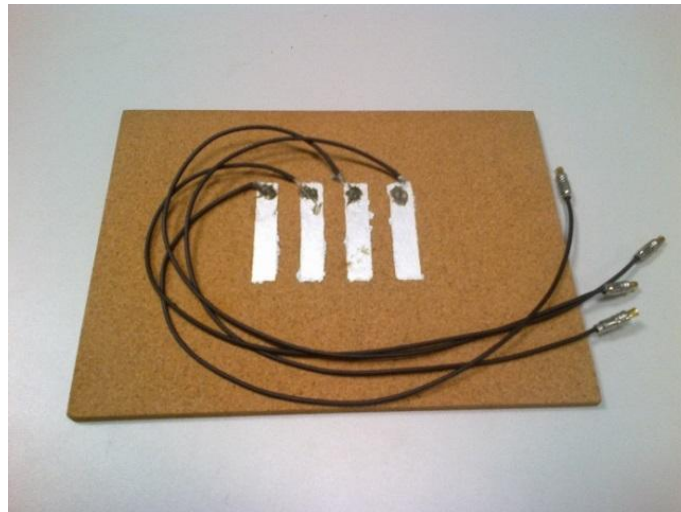


Figure 36: Silver Paint electrodes painted on a P50 plate. Same geometry as configuration four (C4).

The experiment consisted in repeating the same proceeding of section 5.2.4, but just for configuration 4 and now using the silver paint electrodes. The results are shown in Figure 37, where the amplitude and phase values for PCB and silver paint (SP) are compared. It is also shown on Table 6. Unlike the double electrodes present in the PCB design, the silver paint electrodes comprise one layer only.

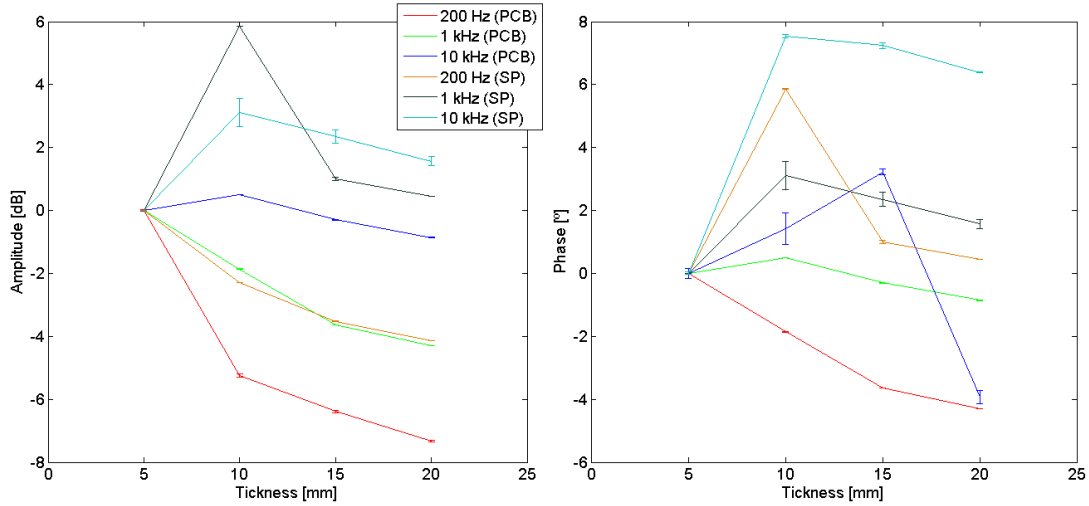


Figure 37: Amplitude and phase as a function of thickness vs. silver paint electrode [29].

		Frequency [kHz]	Thickness [mm]							
			5		10		15		20	
			PCB	SP	PCB	SP	PCB	SP	PCB	SP
Mean	Amplitude [dB]	1	-4.758	3.667	-6.619	9.526	-8.404	4.680	-9.057	4.120
		10	-14.271	-8.750	-13.773	-5.637	-14.571	-6.394	-15.129	-7.181
	Phase [°]	1	335.136	308.230	350.232	313.654	352.571	321.360	352.319	321.842
		10	327.604	321.363	332.115	321.478	334.597	322.249	335.431	320.686
Standard Deviation	Amplitude [dB]	1	0.003	0.005	0.005	0.008	0.002	0.052	0.002	0.006
		10	0.009	0.008	0.007	0.453	0.007	0.213	0.006	0.143
	Phase [°]	1	0.029	0.044	0.009	0.041	0.021	0.278	0.022	0.044
		10	0.043	0.058	0.036	0.768	0.066	0.742	0.074	0.858

Table 6: Average and standard deviation of TPIP measurements for configuration 4: PCB vs. SP electrodes.

We reached the conclusion that, since silver paint electrodes have just one layer, they are more susceptible to external interferences. Thus, they have a lower sensitivity than the PCB electrodes. Nevertheless, silver paint electrodes have several advantages:

- Silver high conductivity;
- Assembling simplicity;
- No restrictions about the shape and dimension of the electrodes;
- Good adhesion to the base material, even in complex surfaces;
- Thermally stable over a wide temperature range.

A blue square graphic with the word 'Chapter' written vertically in white on the left side and a large white number '6' in the center.

Conclusions

This thesis examined the concept of using a non-intrusive sensor to measure ablation during atmospheric entry or re-entry using a mutual impedance technique. Such kind of sensor could have numerous applications, not only in the space domain. The work was performed on Active Space Technologies, Coimbra and the client was ESA.

6.1. Thesis Contribution

This innovative electric sensor can offer real time measurements of TPS thickness during ablation using a low-cost and non-intrusive technique. The data acquired with the sensor can provide inputs for TPS design optimization and mass reduction. Therefore, the sensor can reduce the cost and risk to spaceflight. It is crucial to study and develop a sensor to measure ablative processes in real-time during atmospheric entry and re-entry in view of developing new materials and optimize cost effective techniques.

The prototype fulfilled the initial requirements: low mass, low power, non-intrusiveness, good integration, and good thickness accuracy as described more in detail in Annex 3.

6.2. Looking Forward

This electric sensor can provide relevant technological advancements in TPS optimization both for Mars Sample Return missions and for Asteroid Sample Return missions. Furthermore this technology fits the strategic harmonization roadmaps of ESA and NASA.

A mutual impedance probe operated on a vehicle can be used to create maps of surface ice abundance which would be a valuable tool for the selection of sampling locations for the search of evidence of life in planetary missions.

6.3. Future Work

From an application point of view, the TPIP sensor can be used in entry and re-entry vehicles, in launchers, and eventually in plasma physics in the future. We can see relevant capabilities to study aerothermodynamics and magnetohydrodynamics, but still require significant modeling effort. To study the influence of the plasma on the measurements the sensor must be tested on a reliable testing environment, e.g. Arc jet facility.

Monitoring of heat shield performance is important to investigate aerothermodynamic processes and the interaction between the ablating material and the surrounding plasma. A computational simulation of an atmospheric re-entry would be very interesting to compare with sensor recession thickness measurements.

6.4. Final Thoughts

Silver paint electrodes offer a very simple integration solution. The application is very simple and ensures several advantages, but this solution is more susceptible to noise, leading to a decrease of resolution and sensor efficiency. Future investigation should be conducted to solve this weakness.

From tests in an oven up to 125°C as well as burning and pyrolysis of different media with a blowtorch, it is clear that temperature affects the performance of the electric

sensor. However, it is not obvious which mechanism prevails. Three main sources have been identified: i) modification of medium polarization due to temperature; ii) heating of the electrodes and cables by conduction and convection due to the blowtorch; iii) impact of environmental conditions in the analogue electronics. It was detected a small trend when P50 measurements as a function of thickness have been taken at standard conditions of pressure, temperature, and humidity. These tiny observed variations are due to fluctuations in room temperature (impact on stability of the analogue module) or humidity (effect in the conductivity of the P50 layers). Although producing a small impact in sensor sensitivity, it is likely that resolution can be increased when the source of this variation is identified and corrected.

The presence of plasma on the surface of the medium changes the amplitude and phase measured by the sensor. Even under extreme conditions of induced DC electric and magnetic fields ($E \sim 500 \text{ V m}^{-1}$ and $B \sim 10 \text{ mT}$), small variations could be seen in the amplitude and phase of the signal of the sensor. However, in real space applications it is not expected to find conditions as severe as those tested (e.g. On Earth surface we found $E \sim 100 \text{ V m}^{-1}$ and $B \sim 50 \text{ } \mu\text{T}$ and in the ionosphere and magnetosphere is several orders of magnitude lower). Nonetheless, the situation may be different with AC fields and complementary studies are necessary. In general, amplitude measurements are more accurate than phase measurements. Sensor sensitivity is affected by the length of the cables and is driven by the size of the electrodes. The measurement accuracy archived is better than 0.5 mm for a P50 shield thickness up to 50 mm, as shown in Figure 38.

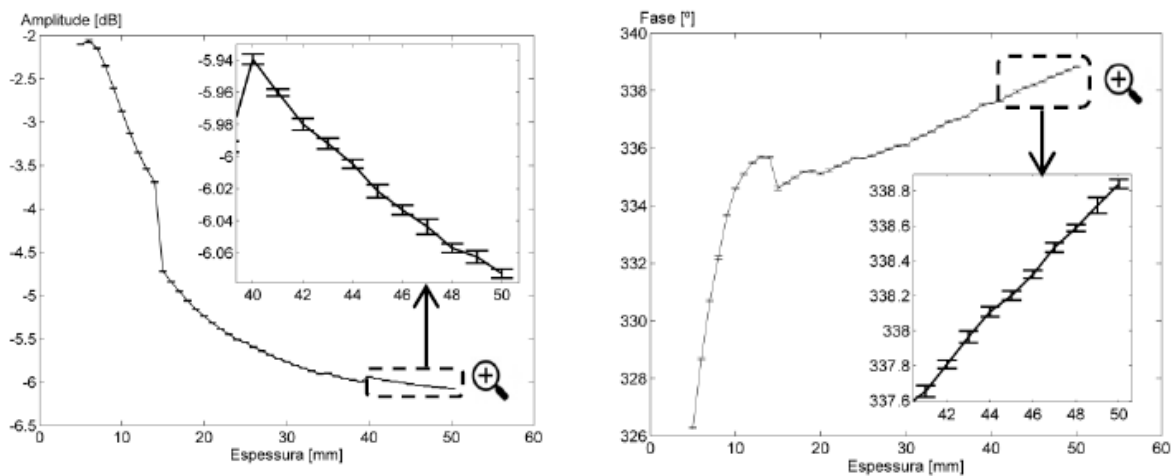


Figure 38: MI signal at 1 kHz as function of P50 thickness [2].

Annexes

A1. P50 data sheet

BRINGING NATURE INTO SPACE

Efficient & Easy integration

Amorim Cork Composites has been manufacturing and supplying a Cork based range of materials, used in Thermal Protection Systems (TPS) for the Aerospace industry, since the beginning of space exploration.

Cork, the bark of the Cork Oak tree (*Quercus Suber*) is nature's foam with a unique combination of properties.

The Cork chemical constituents and structure of the materials make them ideal ablative materials with excellent insulating properties, maintaining low weight to low thermal conductivity results.

The Cork ablative materials work by absorbing a great amount of heat through a phase change. During the phase change, a char layer is formed which acts as an insulator, protecting the inner material and slowing the thermal degradation of the shield while maintaining geometry.

MATERIAL PROPERTIES

	P45	P50	P60
Cork particle size (mm)	1/2	0,5/1	0,5/1
Sheet dimension (mm)	1270x710	1270x710	1000x500
Sheet dimension (inch)	50x28	50x28	40x20
Density @ 20°C ¹	0,32	0,48	0,45
Tensile Strength (psi) ²	125	250	160
Tensile Strength (MPa) ²	0,86	1,50	1,10
Elongation (%) ²	30	13	7
Thermal Conductivity (Btu in)/(h ft ² °F) ³	0,45	0,50	0,55
Thermal Conductivity (W/(m °K)	0,06	0,07	0,08
Specific Heat (Btu/lb °F) ⁴	0,6	0,5	0,4
Specific Heat (KJ/Kg/°K) ⁴	2,5	2,1	1,9
Substrates to bond	Metal and Composite		

(1) ASTM F1315

(2) ASTM F152, Method B

(3) ASTM C177

(4) ASTM C351

Other sheet sizes may be available.

A2. Calcarb data sheet



Calcarb®

**Rigid Carbon Insulation
CBCF 18-2000**



GENERAL

Homogeneous carbon rigid insulation made from carbonised short rayon fibres and designed for high temperature insulation.

TYPICAL APPLICATIONS

Industrial, photovoltaic and CZ furnaces working under vacuum or inert gas upto 3000°C, dependant on system pressure.

CBCF 18-2000 can be provided in a purified form.

Contact sales.hit@mersen.com for further information.

PROPERTIES

	TYPICAL CHARACTERISTICS	
	English Units	SI Units
Bulk Density	11.2 +/- 1.87 lbs/ft ³	0.18 +/- 0.03 g/cm ³
Flexural Strength	149.4 psi	1.03 MPa
Compressive Strength		
// to fiber orientation	159.5 psi	1.10 MPa
⊥ to fiber orientation	110.2 psi	0.76 MPa
Electrical Resistivity	0.30 Ω.in	110,000 μΩ.cm
Coefficient of Thermal Expansion (0 to 1000°C)	1.7 +/- 0.2 x 10 ⁻⁵ /°F	3.0 +/- 0.3 x 10 ⁻⁵ /°C
Expansion (1000 to 2000°C)	1.5 +/- 0.2 x 10 ⁻⁵ /°F	2.6 +/- 0.3 x 10 ⁻⁵ /°C
Water absorption after 6 months in standard conditions	<0.1%	<0.1%
Thermal Conductivity	BTU-Ft/Ft ² Hr°F	W/mK
	Nitrogen / Vacuum	Nitrogen / Vacuum
400°C (750°F)	0.26 / 0.14	0.45 / 0.25
800°C (1470°F)	0.37 / 0.20	0.64 / 0.35
1200°C (2190°F)	0.48 / 0.28	0.84 / 0.48
1600°C (2910°F)	0.66 / 0.40	1.15 / 0.69
2000°C (3630°F)	0.85 / 0.58	1.47 / 1.00
Porosity	89%	89%
Carbon content	>99%	>99%
Residual metallic content standard	<500ppm	<500ppm
purified	<20 ppm	<20 ppm
Temperature treatment	3630°F	2000°C

A3. System Requirements

#	Description
1	The system shall measure the surface recession of the TPS unit employing the MI technique.
2	The proof of concept and preliminary prototype shall test various stimuli profiles in the relevant media.
3	TPIP shall reach TRL 4 “Concept and/or breadboard validation in laboratory environment”

Table 7: Functional Requirements.

#	Description
1	To improve sensor accuracy of various TPS thicknesses and surface profiles, sensor shape optimization analyses shall be carried out, supported by an iterative methodology based in numerical modeling, followed by sensor prototyping and testing
2	The accuracy of the TPS thickness measurement shall not exceed 0.5 mm.
3	The range of measurements can be optimized in accordance with customer needs, by means of controlling the distance between the electrodes.
4	The TPIP sensitivity is mostly constrained by the excitation frequency. For reliable and accurate measurements, the ADC sampling rate of the Rx electrodes should be about 100 times higher than the working frequency.

Table 8: Performance Requirements.

#	Description
1	Concept validation shall test the TPS unit emulating ablation conditions, namely i) high temperatures, ii) electrical fields, iii) magnetic fields, and iv) electrical conducting surface.
2	The sensor shall be able to operate in the range from -50 to + 50 °C.
3	The sensor shall be compatible with the range from -100 to +200 °C.
4	The total required power shall not exceed 0.5 W.

Table 9: Environmental and Operational Requirements.

#	Description
1	The total mass of the electrodes, cables, and analogue unit shall not exceed 0.1 kg.
2	The area occupied by the electrodes depends on the selected arrangement, but shall not exceed 10 cm ² , with a thickness lower than 3 mm.

Table 10: Physical Requirements.

#	Description
1	The TPIP architecture shall be flexible enough to allow multiplexing capabilities if necessary, e.g., multiple sensors sharing signal conditioning and processing.
2	The electrodes shall be attached to the TPS rear end using non-intrusive solutions.

Table 11: Design Requirements and Implementation Constraints.

References

- [1] TPIP Summary Report, SER-TPP-ES-001, Active Space Technologies, 2013.
- [2] F. Simões, A. Mendes, I. Ribeiro, T. Marques, J. Varandas. Method and system for monitoring ablation processes in thermal protection systems. PT 107152N (pending), 2013.
- [3] B. Laub, E. Venkatapatly. Thermal Protection System Technology and facility needs for demanding future Planetary Missions. IPPW1 – Lisbon, 2003.
- [4] J.C. Paulat and P. Boukhobza. Re-entry Flight Experiments Lessons Learned - The Atmospheric Reentry Demonstrator ARD. RTO-EN-AVT-130, EADS – SPACE Transportation, 2007.
- [5] M. Giardino, E. Campagnoli, L. Andrioli, M. Bertone and G. Pippia. Analysis Advances in AblTan Ablative Tool development with application to system model analysis. 26th European Space Thermal Analysis Workshop - ESTEC, Appendix D, 2012.
- [6] F. S. Milos., R. A. Brewer, R. A., Y.-K. Chen, T. H. Squire. Analysis of Galileo Probe Heatshield Ablation and Temperature Data. *Journal of Spacecraft and Rockets*, vol. 36, issue 3, pp. 298-306, 1999.
- [7] J.-M. Bouilly. Thermal Protection System of the HUYGENS Probe for Titan Entry: Qualification, Flight Preparation, and Lessons Learnt. Proceedings form International Planetary Probe Workshop, Greece, July 2005.
- [8] H. Ritter, O. Bayle, Y. Mignot, E. Boulier, P. Portela, J-M. Bouilly, R. Sharda. Ongoing European Developments on Entry Heatshields and TPS Materials. 8th International Planetary Probe Workshop, June 2011.
- [9] Lin, W.-S., Steady Ablation on the Surface of a Two-Layer Composite. *International Journal of Heat and Mass Transfer*, Vol. 48, Nos. 25-26, 2005.
- [10] F. S. Milos and D. J. Rasky. Review of numerical procedures for computational surface thermochemistry. *Journal of Thermophysics and Heat Transfer*, 1994.
- [11] D. Bianchi, F. Nasuti, R. Paciorri, M. Onofri. Computational Analysis of Hypersonic Flows Including Finite Rate Ablation Thermochemistry. 7th European Workshop on Thermal Protection Systems and Hot Structures, ESA-ESTEC, Noordwijk, The Netherlands, 2012.

- [12] D. Bianchi. Modeling of ablation phenomena in space applications. 2007. PhD Thesis, Dept. of Mechanics and Aeronautics, Univ. of Rome “La Sapienza”, Rome, Italy.
- [13] B. Laub, E. Venkatapatly. Current Developments in Future Planetary Probe Sensors for TPS. IPPW1 – Lisbon, 2003.
- [14] F. S. Milos., R. A. Brewer, R. A., Y.-K. Chen, T. H. Squire. Analysis of Galileo Probe Heatshield Ablation and Temperature Data. *Journal of Spacecraft and Rockets*, vol. 36, issue 3, pp. 298-306, 1999.
- [15] Cassanto, J.M., et. Al. A Simple Recession Gage for In Flight Measurement of the Char Degradation Zone for Re-entry Vehicle Heatshields. ISA Sympos-ium, 1980.
- [16] Impedance Measurement Handbook (2nd Edition), Agilent Technologies Co. Ltd., 2003.
- [17] Impedance Measurement Handbook: A guide to measurement technology and techniques, Agilent Technologies, ref. 5950-3000, July 2006.
- [18] E. Barsoukov, J. Macdonald. Impedance Spectroscopy: Theory, Experiment, and Applications. John Wiley & Sons, 2005.
- [19] F. Simões., Résonances des cavités ionosphériques des planètes et de leurs satellites: progrès et perspectives instrumentales. 2007. PhD Thesis, Univ. Pierre et Marie Curie, France.
- [20] M. Hamelin et al. Conductivity and Electron Density Profiles of the Atmosphere of Titan from the Huygens PWA-HASI Instrument: Mutual Impedance Probe Measurements. *Planetary and Space Science*, 55, 1964-1977, 2007.
- [21] R. Grard et al., Electric Properties and Related Physical Characteristics of the Atmosphere and Surface of Titan. *Planetary and Space Science*, 54/12, 1124-1136, 2006 .
- [22] C. A. WALKER AND V. C. HODGES. Comparing Metal-Ceramic Brazing Methods. American welding society, 2008.
- [23] G. Pinaud, A.J. van Eekelen, and J.-M. Bouilly. Aerofast: Development of Cork TPS Material and a 3D Comparative Thermal/Ablation Analysis of an Apollo & a Biconic Sled Shape for an Aerocapture Mission. IPPWC8, June 2011.
- [24] A. Amar, N. Calvert, B. Kirk. Development and Verification of the Charring Ablating Thermal Protection Implicit System Solver. AIAA paper 2011-144, 2011.

- [25] J. M. Cassanto, C. R. Droms and J. Metzger. A Simple Recession Gage for In-flight Measurement of the Char Degradation Zone for Re-Entry Vehicle Heat Shields. 26th International Instrumentation Symposium, Seattle, WA, USA, 1980.
- [26] T. White, I. Cozmuta, J. Santos, B. Laub. MEDLI Aerothermal Environment Reconstruction Efforts. 8th International Planetary Probes Workshop, Portsmouth, VA, USA, 2011.
- [27] D. Empey, E. Martinez. NASA Applications of TPS Instrumentation in Ground and Flight. IPPW9, 2012.
- [28] Fernando Simões, Private Communication, Active Space Technologies, 2013.
- [29] TPIP Final Report, SER-TPP-RP-002, Active Space Technologies, 2013.
- [30] A. Ball, J. Garry, R. Lorenz and V. Kerzhanovich. Planetary Landers and Entry Probes, Cambridge University Press, 2007.
- [31] M. C. Lança et al. Electrical properties of cork and derivatives. Universidade Nova de Lisboa, 2011.
- [32] Atmospheric Reentry Demonstrator. European Space Agency, BR-128, 1998.